Solar Collectors and Solar Hot Water Systems

Runsheng Tang and Guihua Li

Contents

R. Tang (✉) · G. Li
School of Energy and Environment Science, Solar Energy Research Institute, Yunnan Normal University (YNNU), Kunming, China
e-mail: kingtang01@126.com; guihuali688@163.com

R. Wang, X. Zhai (eds.), *Handbook of Energy Systems in Green Buildings*,
https://doi.org/10.1007/978-3-662-49120-1_31

Abstract

In this chapter, solar water collectors and solar water heating systems are addressed. First, the heat transfer inside flat-plate collectors is analyzed; secondly, a detailed mathematical model to calculate collectible radiation on a single tube of a solar tube array is presented, and effects of structural and installing parameters on the performance of evacuated tube solar collectors are investigated. Finally, design of solar water heating systems and their applications in buildings are presented, and an economic comparison between solar water heater, electric heater and gas-fired water heater for hot water supply of buildings in Kunming is made.

Keywords

Solar collector · All-glass evacuated solar tube · Performance analysis · Solar heat gain · Temperature distribution · Annual collectible radiation · Design of solar water heating systems · Passive system · Forced circulation systems · Building integration of solar systems · Economic benefit

Introduction

Among solar energy–based techniques, the solar water heating technique is the only one that has been widely commercialized over the world due to high reliability and economy compared to the conventional water heating systems. A solar water heating system usually consists of solar collectors, water storage tank, pipes, auxiliary heating device, etc. The solar collector, the core element in a solar heating system, is used to transform solar radiation into heat and then transfers the solar heat to fluid flowing through it. Solar collectors are mainly classified into three categories: flat-plate, evacuated tube, and concentrating collectors. Both flat-plate and evacuated tube collectors are generally designed to provide low temperature thermal energy, up to perhaps 100 °C above ambient temperature, and concentrating collectors are usually designed for high temperature solar thermal applications. The fluid used to transfer solar heat of a collector can be air or liquid. The solar collector with air as the heat transfer fluid is usually named as solar air collectors which are generally used for solar drying and building heating, and the one with water as heat transfer fluid is used for water heating systems.

Flat-Plate Solar Collector

Description of Flat-Plate Collectors

To distinguish flat-plate collectors from concentrating collectors, the flat-plate collector is usually termed as that the area of its surface for radiation collection is almost identical to that for solar radiation absorption. Flat-plate collectors use both all beam and diffuse radiation fallen on the collector surface, thus do not require sun-tracking

device. Compared to concentrating collectors, they are simpler in structure, less in maintenance, and more cost-efficient and thus widely used for water and building heating as well industrial process. As shown in Fig. 1, the typical liquid-based flat-plate solar collector, just like a hot box, consists of a solar absorbing plate, back insulation, covers transparent to solar radiation and opaque to the long-wave radiation, tubes for fluid flow to transfer the solar heat away. To improve their thermal performance, the coating with a high absorptance for solar radiation of 0–2.5 μm in wave-length and low emittance for thermal radiation, metal with high thermal conductivity (such as copper and aluminum) as absorbing surface and tubes of fluid flow should be employed.

Heat Transfer in Collectors

Heat transfer inside collectors is in unsteady state due to the variable collectible radiation and climatic conditions. To simplify the analysis and make readers understand how solar radiation transforms into useful heat, equations describing the heat transfer in collectors in the steady-state conditions are presented as follows. The useful heat gain of a solar collector in the steady-state conditions can be simply calculated based on solar heat gain and loss as:

$$Q_u = A_c[S - U_L(T_p - T_a)] \tag{1}$$

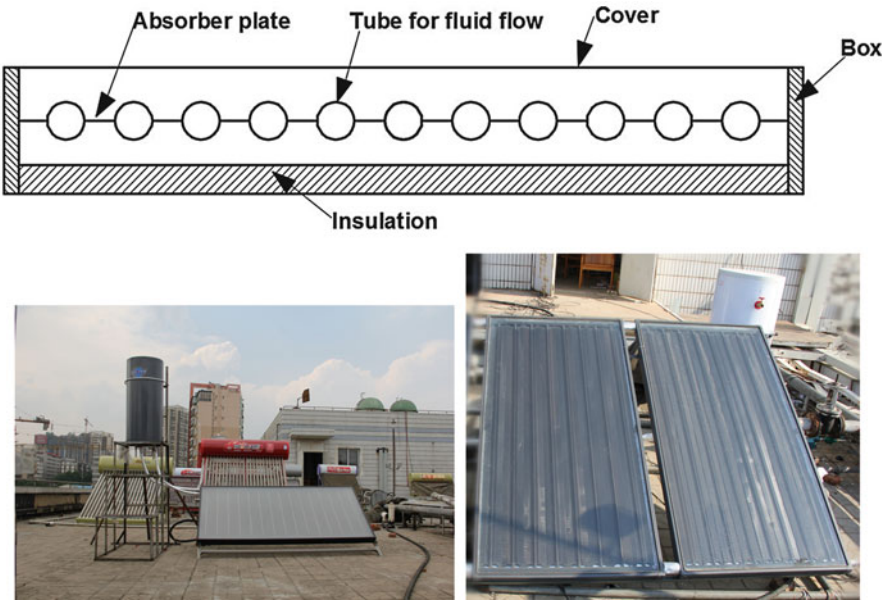

Fig. 1 Cross section of a typical flat-plate solar collector (*up*), photo of collectors (*down*)

where A_c is the area of collectors, $S = (\tau\alpha)I_c$ is the radiation absorbed by unit area of absorbing surface after the incident radiation penetrates the cover, T_p is the mean temperature of absorbing plate, and U_L is the total heat loss coefficient of collectors from the absorbing surface to the ambient air. Given the T_p, the heat transfer from the absorber to the ambient air for the collector with one cover in the steady state can be simply described by the thermal network shown in Fig. 2. It must be noted that the thermal network in this figure already assumes some approximates because it is treated as one-dimension, and edge effects and radiation absorption of cover and thermal capacity of all elements are not considered.

As shown in Fig. 2, heat transfer through the front surface includes radiation loss from the absorber to the cover first then to the sky dome and convective loss from the absorber to the cover first then to the ambient air. Thus, the heat transfer coefficient through the front surface of collector, U_t, can be expressed based on the calculation method of thermal resistance by:

$$U_t = \left[\frac{1}{h_{c,p-c} + h_{r,p-c}} + \frac{1}{h_w + h_{r,c-a}}\right]^{-1} \tag{2}$$

The $h_{c,p-c}$ in Eq. 2 is the convective heat loss coefficient from the absorber to the cover and is related to Nusselt number by:

$$H_{c,p-c} = N_u L/k \tag{3}$$

where L(m) is the distance between plate absorber to the cover, and k (W/m.K) is the thermal conductivity of air. For solar collectors titled β (0–75°) from the horizon, the empirical correlation given by Hollands et al. [1] can be used to estimate N_u as:

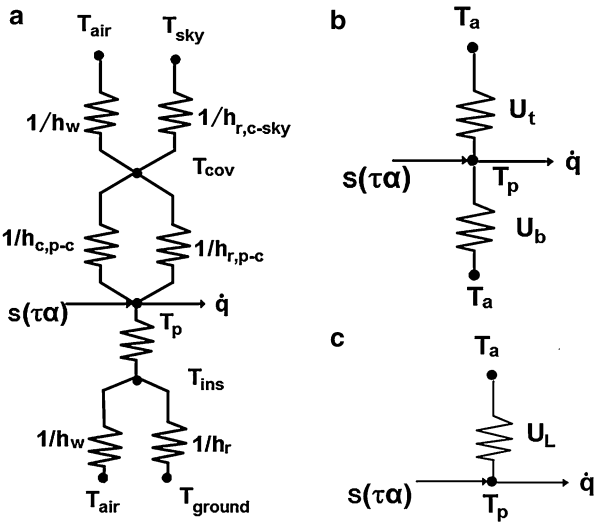

Fig. 2 (**a**) Thermal network of flat-plate collector with one cover; (**b**) equivalent thermal network in terms of top and back heat loss coefficients; (**c**) in terms of total heat loss coefficient

$$N_u = 1 + 1.44\left[1 - 1.44\left[\frac{1.708}{Ra\cos\beta}\right]^+\right]\left[1 - \frac{(\sin 1.8\beta)^{1.6}1708}{Ra\cos\beta}\right] + \left[\left(\frac{Ra\cos\beta}{5830}\right)^{1/3} - 1\right]^+ \quad (4)$$

Where the + superscript indicates that only positive values of terms in the square brackets are used, otherwise it takes to be zero. Since collectors have a finite extent, the ratio of plate length over width, termed as the aspect ratio, may have effect on the heat transfer, thus correction factors on Nusselt should be considered [2]. The $h_{r,p-c}$ in Eq. 2 is the radiative transfer coefficient from the absorber to the cover, and it can be estimated by:

$$h_{r,p-c} = \frac{\sigma\left(T_p^2 + T_c^2\right)(T_p + T_c)}{\left(1/\varepsilon_p + 1/\varepsilon_c - 1\right)} \quad (5)$$

The convective coefficient from the cover to the ambient due to wind is simply estimated by [3]:

$$h_w = 2.8 + 3.0V \quad (6)$$

where v is the wind velocity over the collector surface, and in the case of wind velocity unknown, h_w can be simply set to be 10 W/m^2.K. The $h_{r,c-a}$ is the thermal radiation transfer coefficient calculated based on ambient air temperature due to thermal radiation to the sky dome; thus it is given by:

$$h_{r,c-a} = \frac{Q_{c-sky}}{T_c - T_a} = \frac{\sigma\varepsilon_c\left(T_c^4 - T_{sky}^4\right)f_{c-sky}}{T_c - T_a} \quad (7)$$

where T_{sky} is the sky temperature, a fictitious temperature but useful for calculating thermal exchange between the atmosphere above the ground and surface at the ground level. The sky temperature depends on the vertical distribution of water vapor and atmospheric temperature variation with height near the ground surface [4, 5], and many empirical correlation can be found in the literatures [4, 6]. The atmospheric layer near the ground differs from one place to another. As a result, different places would have different correlations for the calculations of atmospheric radiation. The general expression for sky temperature T_{sky} uses two parameters: the sky emissivityε^{sky} and the ground level air temperature T_a. They are related by

$$T_{sky} = T_a\varepsilon_{sky}^{0.25} \quad (8)$$

The sky emissivity ε^{sky} is often expressed as a function of various parameters. The most commonly used correlations under clear skies were the one suggested by Berdahl and Frombergy [7] based on measured data in three cities in the USA and the one suggested by Berdahl and Martin [8] based on monthly averaged sky measurements in six US cities as follows:

$$\varepsilon^{\mathrm{sky}} = 0.741 + 0.0062\mathrm{T_{dp}} \tag{9}$$

$$\varepsilon^{\mathrm{sky}} = 0.711 + 0.56\left(\mathrm{T_{dp}}/100\right) + 0.73\left(\mathrm{T_{dp}}/100\right)^2 \tag{10}$$

Where T_{dp} is the dew point temperature of air in degrees Celsius. For moist air, the dew point temperature T_{dp} ($0 < T_{dp} < 65$ °C) had the following empirical correlation expressed in degree Celsius [9]:

$$\mathrm{T_{dp}} = 26.13722 + 16.988833\mathrm{a} + 1.04961\mathrm{a}^2 \tag{11}$$

where $a = ln(\varphi P_{sa})$ and P_{sa} (in. Hg) is the saturated vapor pressure of the air at T_a. According to the definition of the dew point temperature, the reversed formula of Eq. 11 can be used to calculate the saturation vapor pressure of the air at any temperature T (°C), that is:

$$\mathrm{P_{sa}} = \exp\left[-8.0929 + 0.97608(\mathrm{T} + 42.607)^{0.5}\right] \ (0 < \mathrm{T} < 65^{\mathrm{o}}\mathrm{C}) \text{ in in.Hg} \tag{12a}$$

$$\mathrm{P_{sa}} = 3385.5\exp\left[-8.0929 + 0.97608(\mathrm{T} + 42.607)^{0.5}\right] \ (0 < \mathrm{T} < 65^{\mathrm{o}}\mathrm{C}) \text{ in N/m}^2 \tag{12b}$$

The saturation vapor pressures calculated in Eq. 12b [10] are in complete agreement with those tabulated by Incropera et al. [11]. The relative humidity φ can be directly measured or calculated based on measured wet-bulb temperature (T_w) and dry-bulb air temperature (T_a) as follows:

$$\mathrm{T_w} = 2.265(1.97 + 4.3\mathrm{T_a} + 104\mathrm{w})^{0.5} - 14.85 \tag{13a}$$

$$\mathrm{P_w} = 29\mathrm{wP_{sa}}/18 \tag{13b}$$

$$\phi = \mathrm{P_w}/\mathrm{P_{sa}} \tag{13c}$$

Where P_w is vapor pressure of the air. Many other correlations based on their own measurements in different countries also have been proposed. One of the simpler formulations is Swinbank's [12]:

$$\mathrm{T_{sky}} = 0.0552T_a^{1.5} \tag{14}$$

The f_{c-sky} is the tilt factor. For a low, uniformly overcast sky, the f_{c-sky} is equal to the view factor of the tilted surface to the sky dome, namely:

$$\mathrm{F}(\beta) = 0.5(1 + \cos\beta) \tag{15}$$

For a clear sky, the tilt factor can be written in terms of a polynomial fit [9]:

$$\mathrm{F}(\beta) = 1 + 0.02725\beta - 0.2524\ 2\beta + 0.03372\ 3\beta \tag{16}$$

where the β is the tilt-angle from the horizon in radians.

Given T_p, T_c, T_a, and T_{sky}, the top loss coefficient U_t can be calculated based on Eqs. 2, 3, 4, 5, 6, and 7. But in the practical calculations, the cover temperature T_c is not usually known; therefore, iterative calculations must be used based on assumed initial value of T_c. Unfortunately, such general procedure of calculations is time consuming even on a computer. To simply calculations, Klein [13] developed an empirical correlation as follows [2]:

$$U_t = \left[\frac{N}{\frac{C}{T_p}\left(\frac{T_p - T_a}{N+f}\right)_e} + \frac{1}{h_w}\right]^{-1} + \frac{\sigma\left(T_p - T_a\right)\left(T_p^2 + T_a^2\right)}{\left(\varepsilon_p + 0.00591Nh_w\right)^{-1} + \frac{2N + f - 1 + 0.133\varepsilon_p}{\varepsilon_c} - N} \tag{17}$$

where N: number of covers

$$f = \left(1 + 0.0892h_w - 0.1166h_w\varepsilon_p\right)\left(1 + 0.07866N\right)$$

$$C = 520\left(1 - 0.000051\beta^2\right) \text{ for } 0^o < \beta < 70^o, \text{and } \beta = 70^o \text{ for } \beta > 70^o$$

$$e = 0.43\left(1 - 100/T_p\right)$$

β = collector tilt in degree
ε_c: emissivity of cover (0.88 for glass)
ε_p: emissivity of absorber plate
T_p: mean temperature of absorber plate (K)
T_a: ambient temperature (K)
h_w: convective coefficient of wind (W/m^2 K)

The energy loss through the bottom of collectors is a result of heat conduction through back insulation first then dissipating to the ambient air by convection and thermal radiation, and it can be approximately represented by the resistance of heat conduction through back insulation because the magnitude of both convective and radiative resistances is usually much small compared to that of heat conduction through the insulation. Thus, one has:

$$U_b = \frac{k}{L} \tag{18}$$

where k and L are the thermal conductivity and thickness of back insulation, respectively. It must be noted that the overall heat loss should include the heat loss through the edges of collectors and can be simply estimated by:

$$U_e = \frac{(UA)_{edge}}{A_c} \tag{19}$$

Therefore, the overall heat loss coefficient is calculated by:

$$U_L = U_t + U_b + U_e \tag{20}$$

One must note that the accurate calculation of radiation absorbed by plate of collector in terms of $S = (\tau\alpha)I_T$ is quite complicated because the collectible radiation on the cover of collectors includes beam and sky diffuse radiation on the one hand, and incident radiation on the way to the absorber undergoes multiple reflection and absorption within the cover and in between the cover and absorber plate; furthermore, the solar transmittance of the cover is the angular dependence [2].

It is known from Eq. 1 that, given the overall heat loss (U_L) and mean temperature of absorber of collectors (T_p), the useful solar gain can be simply calculated. However, the measurement of T_p is quite difficult in practice, and the measurement of fluid temperature in a collector is much easy. In the following section, the task is to find the relationship between T_p and mean fluid temperature in tube (T_f).

Heat Transfer from the Absorber Plate to Tubes

Given a solar collector, the useful heat gain depends on mean temperature of the absorber plate based on Eq. 1, and the temperature distribution of the absorber in between tubes depends on the heat transfer from plate to tubes for the sheet-tube/fin-tube absorber. So to find the T_p of absorber, it is necessary to determine the temperature distribution of absorber between tubes. In the following section, heat transfer from plate to tube for sheet-tube absorber is analyzed.

As shown in Fig. 3, the distance between tubes is W, the tube diameter is D, and the thickness of sheet is δ. It is known from the knowledge of heat transfer that the heat flux through the sheet's centerline between tubes is zero; thus, the region from the centerline to tube base is selected for the analysis. The energy balance equation for finite element of width Δx and unit length in the flow direction is expressed by:

$$S\Delta x - U_L\Delta x(T - T_a) + \left(-k\delta\frac{dT}{dx}\right)|_x - \left(-k\delta\frac{dT}{dx}\right)|_{x+\Delta x} = 0 \tag{21}$$

Dividing by Δx and finding the limit as Δx approaches zero obtains

$$\frac{d^2T}{dx^2} = \frac{U_L}{k\delta}\left(T - T_a - \frac{S}{U_L}\right) \tag{22}$$

The boundary conditions necessary to solve this second-order differential equation are:

$$\frac{dT}{dx}|_{x=0} = 0, T(x = 0.5(W - D)) = T_b \tag{23}$$

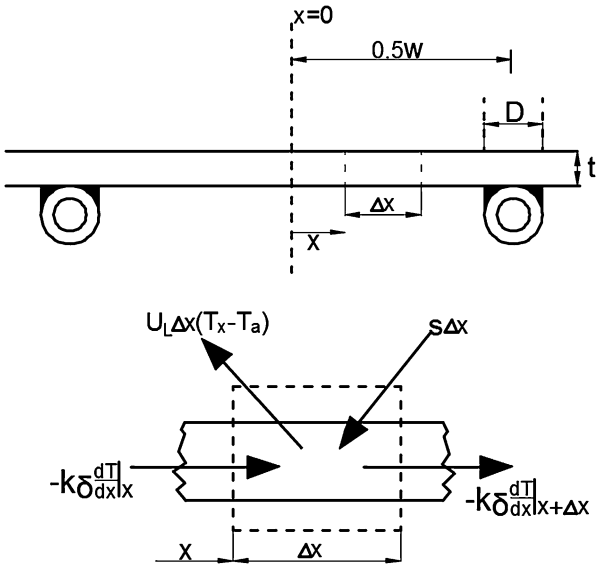

Fig. 3 Configuration of sheet-tube absorber (*up*); energy balance on a finite element (*down*)

where T_b is the temperature of fin base at the tube. Substituting boundary conditions into the general solution of Eq. 22 yields:

$$\frac{T - T_a - S/U_L}{T_b - T_a - S/U_L} = \frac{\cosh mx}{\cosh m(W-D)/2} \tag{24}$$

where m=$U_L/k\delta$, thus the energy conducted to tube from both left and right fins is as:

$$q_{fin} = -2k\delta \frac{dT}{dx}\Big|_{x=0.5(W-D)} = (W - D)[S - U_L(T_b - T_a)] \frac{\tanh m(W-D)/2}{m(W-D)/2} \tag{25}$$

or

$$q_{fin} = (W - D)F[S - U_L(T_b - T_a)] \tag{26}$$

where $F = \frac{\tanh m(W-D)/2}{m(W-D)/2}$ is the fin efficiency of fins. The useful heat gain of a tube for unit length in the direction of flow includes heat gain from both left and right fins (q_{fin}), and the heat gain due to direct solar irradiation on the tube thus is given by:

$$q_u = q_{fin} + D[S - U_L(T_b - T_a)] = [(W - D)F + D][S - U_L(T_b - T_a)] \tag{27}$$

The useful heat gain of tubes must be finally transferred to the fluid; therefore, q_u also can be expressed by:

$$q_u = \frac{T_b - \overline{T}_f}{\frac{1}{h_f \pi D_i} + \frac{1}{C_b}} \tag{28}$$

where D_i is the inner diameter of the tube and h_f is the convective coefficient of fluid inside the tube, C_b is the bond conductance. Substituting T_b obtained from Eq. 27 into Eq. 27 yields

$$q_u = WF'\left[S - U_L\left(\overline{T}_f - T_a\right)\right] \tag{29}$$

where F' is termed as efficiency factor of the collector and given by:

$$F' = \frac{1}{\frac{WU_L}{\pi D_i h_f} + \frac{WU_L}{C_b} + \frac{W}{D + (W - D)F}} \tag{30}$$

Assuming that the collector consists of n tubes with length of L, the useful heat gain of the collectors is approximately given by (setting $A_c = nWL$ as the collector area):

$$Q_u = A_c F'\left[S - U_L\left(\overline{T}_f - T_a\right)\right] \tag{31}$$

Compared to Eq. 1, the F' can be explained that represents the ratio of the actual useful energy gain of collector to the useful gain that would result if the absorber of collector was kept at the mean fluid temperature (T_f). It depends on the construction of the collector but is practically independent on operating condition; therefore, different geometry of the absorber would yield different F'. The Eq. 30 is merely suitable for the calculating F' of sheet-tube absorber. Two typical absorbers as shown in Fig. 4 are very common in the market of solar collectors. For fin-tube absorber as shown in Fig. 4a, F' is given by:

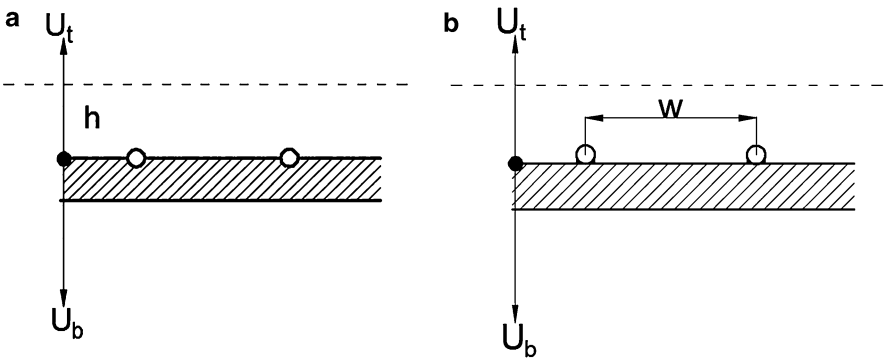

Fig. 4 (**a**) Fin-tube absorber; (**b**) tube-sheet absorber

$$F' = \frac{1}{\frac{WU_L}{\pi D_i h_f} + \frac{W}{D + (W - D)F}} \tag{32a}$$

And for sheet-tube absorber (tubes are welded on front side of the sheet as shown in Fig. 4b)

$$F' = \frac{1}{\frac{WU_L}{\pi D_i h_f} + \frac{1}{\frac{D}{W} + \frac{1}{\frac{WU_L}{C_b} + \frac{W}{(W - D)}}}} \tag{32b}$$

If the temperature rise inside tube along the flow direction is small, the mean fluid temperature can be simply estimated from temperatures of fluid at the inlet and outlet of collectors:

$$\overline{T}_f = 0.5\left(T_{f,i} + T_{f,o}\right) \tag{33}$$

then the useful solar gain of collectors is simply estimated based on Eq. 28. But Eq. 33 for the calculation of $\overline{T}_f$ is not appropriate in practice because the fluid temperature does not linearly increase along the flow direction as seen in the following section.

Temperature Distribution of Fluid in Flow Direction

To be convenient for the calculation of useful heat gain, it is necessary to find the mean temperature of fluid based on fluid temperature at the inlet which can be directly measured. As shown in Fig. 5, the solar gain obtained by the finite element Δy of a single tube is ultimately transferred to the fluid flowing through it, thus one has:

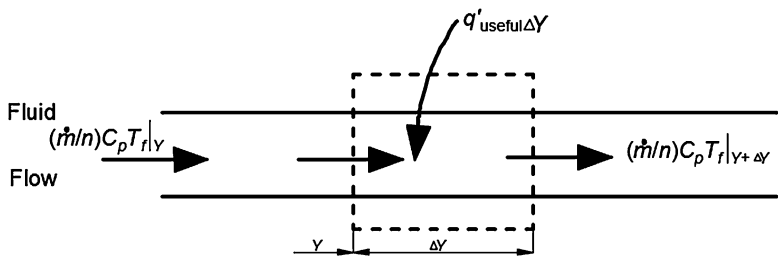

Fig. 5 Energy balance on fluid element

$$\left(\frac{\dot{m}}{n}\right)\mathrm{C_p T_f}\big|_y - \left(\frac{\dot{m}}{n}\right)\mathrm{C_p T_f}\big|_{y+\Delta y} + \Delta y\, q_u = 0 \tag{34}$$

where $\dot{m}$ is the mass flow rate through the collector which consists of N tubes. Dividing by Δy and finding the limit as Δy approaches zero, and substituting Eq. 29 for q_u obtains:

$$\dot{m}C_p \frac{dT_\mathrm{f}}{dy} - \mathrm{nW}F'[\mathrm{S} - \mathrm{U_L}(\mathrm{T_f} - \mathrm{T_a})] = 0 \tag{35}$$

Assuming $\mathrm{U_L}$ is independent of fluid temperature, the fluid temperature at any position y (at $\mathrm{y} = 0$, $\mathrm{T_f} = \mathrm{T_{f,i}}$) is expressed by:

$$\frac{\mathrm{T_f} - \mathrm{T_a} - S/U_L}{\mathrm{T_{f,}}_i - \mathrm{T_a} - S/U_L} = \exp\left(-U_L nWF' y/\dot{m}C_p\right) \tag{36}$$

The outlet fluid temperature is obtained by setting $\mathrm{y} = \mathrm{L}$ and $\mathrm{A_c} = \mathrm{nWL}$ as:

$$\frac{\mathrm{T_{f,}}_o - \mathrm{T_a} - S/\mathrm{U_L}}{\mathrm{T_{f,}}_i - \mathrm{T_a} - S/\mathrm{U_L}} = \exp\left(-A_c \mathrm{U_L} F'/\dot{m}C_p\right) \tag{37}$$

And the mean temperature of fluid along the tubes is given by:

$$\begin{aligned}\overline{\mathrm{T}}_\mathrm{f} &= \frac{\int_0^L \mathrm{T_f} dy}{L} \\ &= (\mathrm{T_a} + \mathrm{S/U_L}) + \frac{\mathrm{T_{f,}}_i - T_a - S/\mathrm{U_L}}{A_c \mathrm{U_L} F'/\dot{m}C_p}\left[1 - \exp\left(-A_c \mathrm{U_L} F'/\dot{m}C_p\right)\right.\end{aligned} \tag{38}$$

Substituting above equation into Eq. 31 for $\overline{\mathrm{T}}_\mathrm{f}$ obtains

$$Q_u = \mathrm{A_c F_R}\left[\mathrm{S} - \mathrm{U_L}\left(\mathrm{T_{f,i}} - \mathrm{T_a}\right)\right] \tag{39}$$

where $\mathrm{F_R}$ is termed as heat removal factor of collectors and is given by:

$$F_R = \frac{\dot{m}\mathrm{C_p}}{A_c \mathrm{U_L}}\left[1 - \exp\left(-A_c U_L F'/\dot{m}\mathrm{C_p}\right)\right] \tag{40}$$

The $\mathrm{F_R}$ can be explained as the ratio of actual heat transfer to the maximum possible heat transfer. The maximum heat transfer (solar gain) occurs when whole collector is at the inlet fluid temperature because heat loss to the ambient air is the minimum. It must be noted that $\mathrm{F_R}$ depends on structure of collectors but also on operating condition such as fluid mass flow rate. In practical applications, $\mathrm{F_R}(\tau\alpha)$ and $\mathrm{F_R U_L}$ of a collector are usually obtained by testing its efficiency line under steady-state operating conditions.

Analysis in the above indicates that, given the structure of a flat-plate collector and operation conditions, the thermal performance is dependent on the $k\delta$, product of thickness and heat conductivity of the absorber, indicating that flat-plate solar collector with identical $k\delta$ would have identical thermal performance. As an example, copper and aluminum are widely used as fin-tube absorber of flat-plate collectors. To make the thermal performance of both collectors made of copper and aluminum identical, only a half thickness of aluminum absorber is required for copper absorber as the thermal conductivity of copper is about two times of that of aluminum, but the cost of copper absorber is about 3.5 times of aluminum absorber because the price of copper is 2.5 times that of aluminum and the density of copper is about three times of aluminum.

All-Glass Evacuated Solar Collector

Description of Evacuated Solar Collectors

Because of high heat loss coefficient, ordinary flat-plate collectors are not practical for high temperature applications, say above 80 °C. When higher temperatures are desired, one needs to reduce the heat loss from the absorber of collectors to the ambient air. This can be accomplished principally by two methods: evacuation and concentration, either singly or in combination. The natural configuration for an evacuated collector is the glass tube. There are many possible designs, but all of them use glass envelope for radiation transmitting and selective coatings on the absorber for the reduction of thermal radiation loss at high temperature. The basic problems for the designs of evacuated collectors arise from the thermal expansion of the absorber relative to the glass tube and enclosing the absorber within the glass tube. Evacuated collectors are broadly classified into two types based on the material used to construct the absorber: metal-glass evacuated tube and all-glass evacuated tube. As shown in Fig. 6, the metal-glass evacuated collector consists of a metal absorber with a tube or U-tube for the heat removal, metal-glass sealed at the one end to make metal absorber thermally extend and shorten. The production of metal-glass evacuated collectors is complex technically due to the difficulty of metal-glass sealing and high cost; thus, quite a few manufacturers are offering such collector for sale.

All-glass evacuated solar tube (ET), first developed by Owens-Illinois Co. in 1970s, consists of two concentric tubes sealed at one end with an annular vacuum space and a selective surface absorber on the out surface (vacuum side) of the inner tube as shown in Figs. 7 and 8. ET is usually made from borosilicate glass with the main glass-forming constituents silica and boron oxide. Borosilicate glasses are most well known for having very low coefficient of thermal expansion (less than 3.3×10^{-6} m/m.°C is required for ET), making them resistant to thermal and mechanical shock more than any other common glass. To reduce heat loss by thermal radiation, solar selective coating is required, and metal-ceramic composites are of special interest because of thermal stability at high temperature. Cermets usually

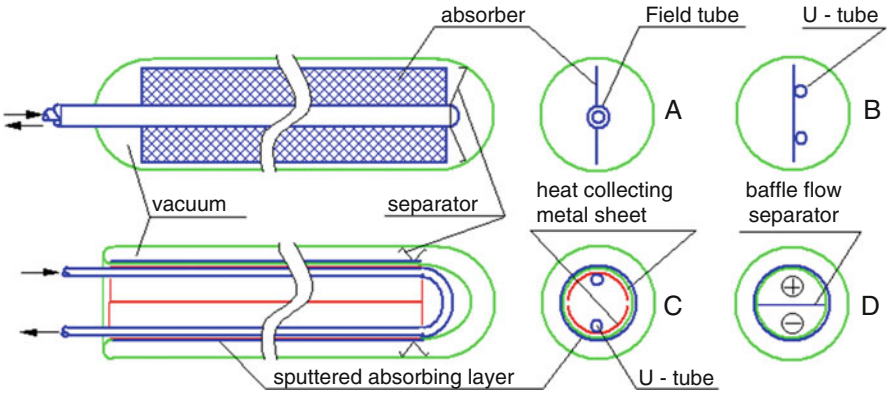

Fig. 6 (**a**, **b**) Metal-glass evacuated collector, (**c**) all-glass evacuated tube with inserted sheet-finned U-tube, (**d**) all-glass evacuated tube with inserted baffle flow separator

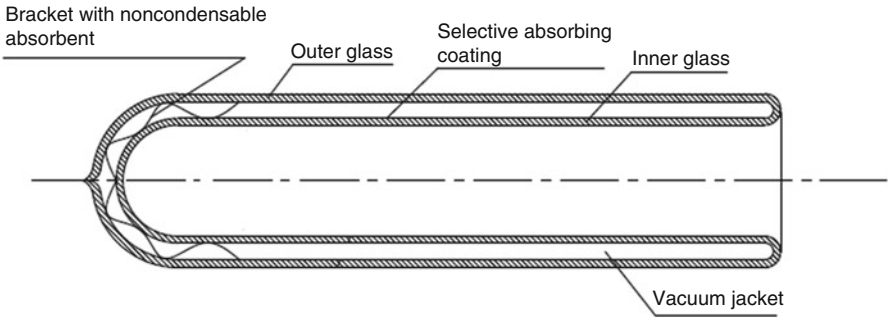

Fig. 7 Geometry of all-glass evacuated tube

consist of nanometer-sized metal particles embedded in a ceramic binder. For better performance of solar selective absorbers, multilayer cermets with different metal content in each of sublayer is sandwiched between an antireflection layer and an thermal infrared reflector layer as shown in Fig. 9. To date, various metal-ceramic composites were reported and prepared by magnetron sputtering [14]. Among these cermets, stainless steel-aluminum nitride (SS-AlN) and aluminum-aluminum nitride (Al-AlN) have been widely adopted for the production of all glass evacuated solar tubes in China. A number of studies indicated that the coating with two cermet layers provided the best optical results as indicated by Liu and Tang [15] and Zhang [14]. In addition, the annular space between inner and outer tubes of ET must be evacuated with the pressure in the magnitude of 10^{-3} Pa for good thermal insulation (Fig. 10).

In practical applications, solar tubes can be horizontally arranged or tilt-arranged to form a solar collector. For domestic solar water heaters (i.e., water-in-glass evacuated tube solar water heaters), solar tubes are usually tilt-arranged with their opening ends being directly inserted into the storage tank (referred to as T-type collector in this chapter), whereas for large-scale solar heating systems, solar tubes

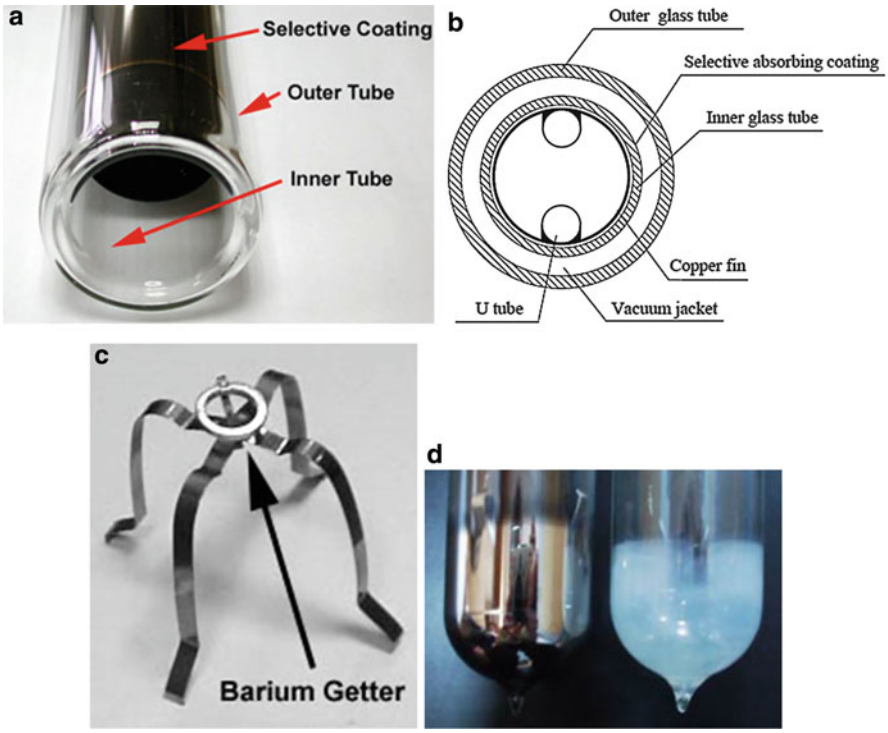

Fig. 8 (**a**) Open end of all-glass evacuated tube, (**b**) cross section of ET with inserted U-tube (**c**) bracket with barium getter, (**d**) *left*: gas absorbing coating deposited on the sealed end; *right*: gas absorbing coating after tube being filled with air

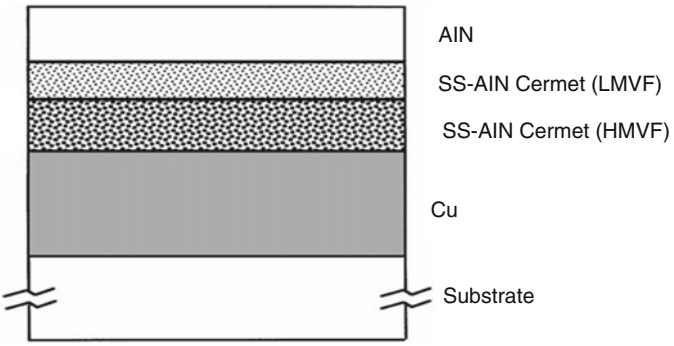

Fig. 9 Configuration of SS-AlN cermet solar selective absorbers

are horizontally arranged (referred to as H-type collector) with their opening ends being directly inserted into manifolds, as seen in Fig. 11. To increase energy collection, a diffuse flat reflector (DFR) is equipped behind solar tubes to reflect the incident radiation through gaps between tubes to solar tubes. But collectors with

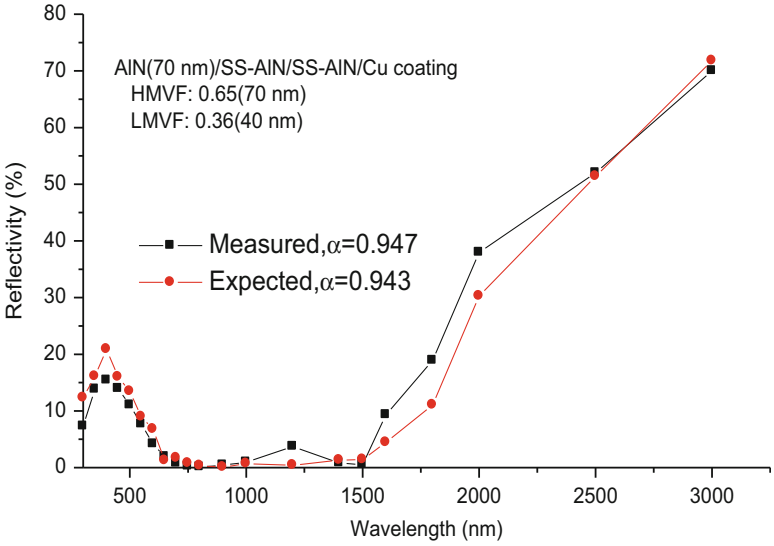

Fig. 10 Reflective solar spectrum of a typical SS-AlN coating (From Liu and Tang [15])

Fig. 11 *Left*: H-type collector; *right*: T-type collector (Courtesy of Xinyuan Sunlight Co., Yunnan of China)

DFR were found to be easily damaged due to the deposit of snow on DFR in winters or the wind-induced force on DFR in summers.

Daily Radiation Received by Solar Tube Collectors

Coordinate Systems for Positioning the Sun

Unlike flat-plate collectors, the calculation of radiation received by a single solar tube of a collector is extremely complex. To perform this work, it is essential to determine the position of the sun in the sky dome. The position of the sun in the sky

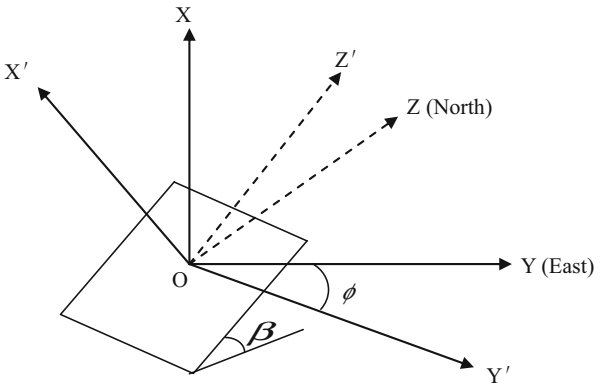

Fig. 12 Coordinate systems used for positioning the sun

dome is usually described by the terrestrial horizon coordinate system, in which, X-axis points to the top of the sky dome, Y-axis points to due east, and Z-axis points to due north (see Fig. 12). In this coordinate system, the unit vector from the earth to the sun can be expressed by [16]:

$$\mathbf{n}_s = \left(n_x, n_y, n_z\right) \tag{41}$$

where

$$n_x = \cos\delta\cos\lambda\cos\omega + \sin\delta\sin\lambda \tag{42a}$$

$$n_y = -\cos\delta\sin\omega \tag{42b}$$

$$n_z = -\cos\delta\sin\lambda\cos\omega + \sin\delta\cos\lambda \tag{42c}$$

where λ is the site latitude, ω is the hour angle, δ is the declination and determined by the day of a year as:

$$\sin\delta = -\sin 23.45\cos\left[360(n+10)/365.25\right] \tag{43}$$

where n is the number of days counted from the first day of a year.

It is assumed that the collectors are mounted with tilt-angle, β, from the horizon and azimuth angle, φ, measuring from due south to west. To be convenient for calculations, a new coordinate system was suggested that the $Y'OZ'$coordinate plane lies on the surface of collectors with X′axis normal to the collector surface and pointing to the southern sky dome, Y′axis is parallel to the horizon and points to southeast, φ from the east, and Z′axis points to the northern sky dome, as seen in Fig. 12. In the suggested coordinate system, the unit vector from the earth to the sun can be obtained based on the technique of coordinate system transformation as follows:

$$\mathbf{n}_s' = \left(n_x', n_y', n_z'\right) \tag{44}$$

where

$$n'_x = n_x \cos\beta - \left(n_y \sin\varphi + n_z \cos\varphi\right) \sin\beta \tag{45a}$$

$$n'_y = n_y \cos\varphi - n_z \sin\varphi \tag{45b}$$

$$n'_z = n_x \sin\beta + \left(n_y \sin\varphi + n_z \cos\varphi\right) \cos\beta \tag{45c}$$

For a solar tube collector with DFR, the collectible radiation on a single tube of the solar collector at any moment includes four components: beam radiation directly intercepted by the tubes, diffuse radiation directly intercepted by the tubes, radiation reflected from DFR due to the irradiation of beam radiation through gaps between solar tubes, and that reflected from DFR due to the irradiation of sky diffuse radiation through gaps between solar tubes.

Beam Radiation Directly Intercepted by a Single Tube

The beam radiation directly intercepted by unit length of a single tube is expressed by:

$$I_{bt} = D_1 \mathrm{I_b} \cos\theta_t f(\Omega) \tag{46}$$

where D_1 is the diameter of inner tube of the solar tube, I_b is the instantaneous beam radiation intensity on a surface normal to radiation, θ_t is the incident angle of solar rays on the intercepting plane of solar tube, namely the angle formed by solar ray and the projection of solar ray on the cross section of solar tube, because the normal of intercepting plane of tubes for solar rays overlays the projection of solar rays on the cross section of solar tubes as shown in Fig. 13. $\cos\theta_t$ in Eq. 46 is determined by dot product between $\mathbf{n}_s{}'$ and unit vector of intercepting plane (i.e., projection of solar ray on the cross section of the tube). For T-type collectors, it is given by:

$$\begin{aligned}\cos\theta_t &= \mathbf{n}_s{}' \bullet \mathbf{n}_{s,p} = \left(n'_x, n'_y, n'_z\right) \bullet \left(n'_x, n'_y, 0\right) / \sqrt{n'_x n'_x + n'_y n'_y} \\ &= \sqrt{n'_x n'_x + n'_y n'_y}\end{aligned} \tag{47a}$$

Similarly, for H-type collectors, $\cos\theta_t$ is determined by

$$\cos\theta_t = \sqrt{n'_x n'_x + n'_z n'_z} \tag{47b}$$

$f(\Omega)$ in Eq. 46 is the interception factor of solar tubes for solar rays due to shading each other between adjacent tubes, and related to Ω, the angle formed by the projection of solar ray on the cross section of the tube and the normal of the collector surface as shown in Fig. 13. For T-type collectors, angle, Ω, is determined by:

$$\tan\Omega = \left|\frac{n'_y}{n'_x}\right| \tag{48a}$$

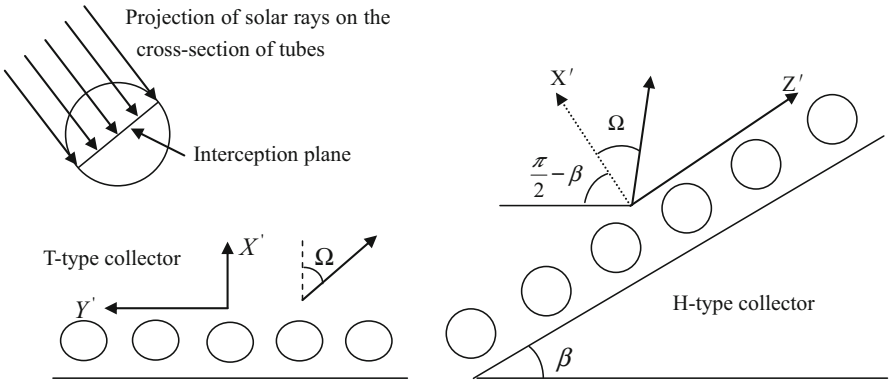

Fig. 13 Cross section of both T- and H-collectors

Whereas for H-type collectors,

$$\tan\Omega = \left|\frac{n_z'}{n_x'}\right| \tag{48b}$$

Knowing angle Ω, the $f(\Omega)$ is given by:

$$f(\Omega) = \begin{cases} 1 & \Omega \le \Omega_0 \\ \dfrac{B}{D_1}\cos\Omega + 0.5\left(1 - \dfrac{D_2}{D_1}\right) & \Omega_0 < \Omega \le \Omega_1 \\ 0 & \Omega \ge \Omega_1 \end{cases} \tag{49}$$

In the above expression, $f(\Omega)$ is also set to be 0 when $n_x^{'} \le 0$, implying no beam radiation incident on the surface of collectors. As shown in Fig. 14, critical angles Ω_0 and Ω_1 are calculated by:

$$\cos\Omega_0 = \frac{D_1 + D_2}{2B} \tag{50a}$$

$$\cos\Omega_1 = \frac{D_2 - D_1}{2B} \tag{50b}$$

where D_2 is the diameter of cover tube of the solar tube and B is the central distance between two adjacent tubes.

Sky Diffuse Radiation Directly Intercepted by a Single Tube

Assuming the distribution of sky diffuse radiation on the plane coplanar with the cross section of solar tubes is isotropic, radiation from $d\Omega$ and intercepted by unit length of a tube can be expressed by:

$$dI_{dt} = D_1 \ \text{if}(\Omega)d\Omega \tag{51}$$

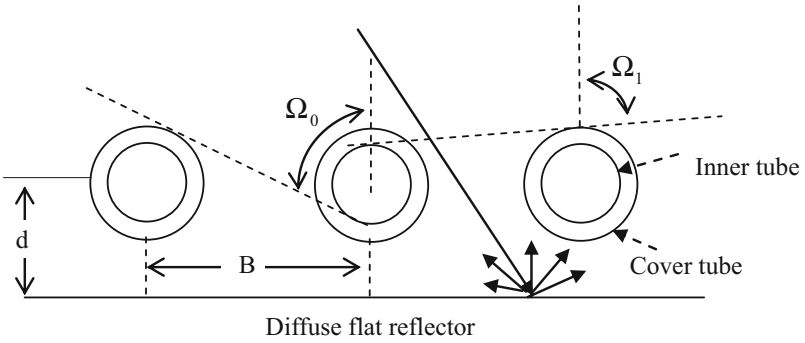

Fig. 14 Critical angles of solar rays for radiation interception

where i is the directional intensity of sky diffuse radiation on the plane coplanar with the cross section of tubes and can be determined by summing radiation from all direction on the plane, namely:

$$\int_{-0.5\pi}^{0.5\pi} i\cos\Omega d\Omega = I_{d\beta} \tag{52}$$

and leading to $i = 0.5I_{d\beta}$. For T-type collectors, $I_{d\beta}$ is the sky diffuse radiation on the collector surface, i.e., $I_{d\beta}$=0.5(1+cosβ)I_d; whereas for H-type collectors, $I_{d\beta}$ is the sky diffuse radiation on the horizonI_d, i.e., $I_{d\beta}$=I_d.

Therefore, sky diffuse radiation directly intercepted by unit length of a tube can be obtained by integrating Eq. 51 over the projection angle Ω:

$$I_{dt} = D_1 \int if(\Omega)d\Omega = D_1\pi I_{d\beta}F_{T-S} \tag{53}$$

where F_{T-S}=$\frac{0.5}{\pi}\int f(\Omega)d\Omega$ is termed as the shape factor for diffuse radiation from a tube to the sky.

For T-type collectors, $I_{d\beta} = 0.5(1 + \cos\beta)I_d$, and angle Ω varies from $-\frac{\pi}{2}$ to $\frac{\pi}{2}$ (see Fig. 13); thus, F_{T-S} can be obtained by substituting Eq. 49 into Eq. 53 for f(Ω)and then integrating:

$$\begin{aligned} F_{T-S} &= \frac{1}{\pi}\int_0^{\frac{\pi}{2}} f(\Omega)d\Omega \\ &= \left[\Omega_0 + 0.5\left(1 - \frac{D_2}{D_1}\right)(\Omega_1 - \Omega_0) + \frac{B}{D_1}(\sin\Omega_1 - \sin\Omega_0)\right]/\pi \end{aligned} \tag{54}$$

For H-type collectors, as seen in Fig. 13, $I_{d\beta} = I_d$, angle Ω in Eq. 53 varies from $-\left(\frac{\pi}{2} - \beta\right)$ to $\frac{\pi}{2}$; thus, the shape factor, F_{T-S}, is calculated by:

$$\begin{aligned}\pi F_{T-S} &= 0.5\left[\int_0^{0.5\pi} f(\Omega)d\Omega + \int_0^{0.5\pi-\beta} f(\Omega)d\Omega\right] \\ &= 0.5\left[\Omega_0 + 0.5\left(1-\frac{D_2}{D_1}\right)(\Omega_1-\Omega_0) + \frac{B}{D_1}(\sin\Omega_1 - \sin\Omega_0)\right] + 0.5C_0\end{aligned} \tag{55}$$

where

$$C_0 = \begin{cases} \Omega_0 + 0.5(1-D_2/D_1)(\Omega_1-\Omega_0) + B(\sin\Omega_1 - \sin\Omega_0)/D_1 & 0.5\pi-\beta \geq \Omega_1 \\ \Omega_0 + 0.5(1-D_2/D_1)(0.5\pi-\beta-\Omega_0) + B(\cos\beta - \sin\Omega_0)/D_1 & \Omega_0 \leq 0.5\pi-\beta < \Omega_1 \\ 0.5\pi-\beta & 0.5\pi-\beta \leq \Omega_0 \end{cases} \tag{55a}$$

Radiation Reflected from the DFR Due to the Irradiation of Beam Radiation Through Gaps Between Solar Tubes

It is assumed that the collector array consists of N solar tubes, and N is very large so that the side effect of the collector array can be neglected, thus radiation reflected from all strips ($N-1$ strips in total) on DFR irradiated by beam radiation through gaps and received by unit length of a single tube can be calculated by [17]:

$$I_{wt} = (N-1)I_b\cos\theta_c\rho W F_{w-T}F_{D_2-D_1}/N \approx I_b\cos\theta_c\rho W F_{w-T}\frac{D_1}{D_2} \tag{56}$$

where ρ is the reflectivity of DFR, θ_c is the incident angle of solar rays on the collector surface and determined by:

$$\cos\theta_c = \mathbf{n}_s{}' \bullet \mathbf{n}_c = \left(n_x', n_y', n_z'\right) \bullet (1,0,0) = n_x' \tag{57}$$

F_{w_T} in Eq. 56 is the radiative shape factor from one strip on DFR to all tubes of the collector, $F_{D_2-D_1}$ is the shape factor from cover tube to inner tube of a solar tube and is equal to D_1/D_2, and w is the width of the strip irradiated by beam radiation through gaps between two adjacent tubes as shown in Fig. 15 and calculated by [17]:

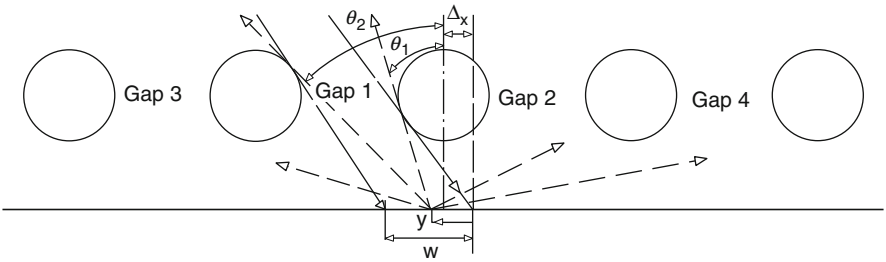

Fig. 15 Reflection from the strip irradiated by beam radiation through a gap

$$w = B - \frac{D_2}{\cos \Omega} \tag{58}$$

By setting w = 0, one obtains the critical angle, Ω_2, as follows:

$$\cos \Omega_2 = \frac{D_2}{B} \tag{59}$$

The shape factor, F_{w-T}, is related to B, distance from center of tube to DFR, d, and projection angle, Ω. When the projection angle, Ω, is larger than critical angle, Ω_2, no beam radiation reaches the DFR, and the shape factor, F_{w-T}, is set at zero at this moment.

Theoretically, radiation reflected from a irradiated strip can escape into the sky through all gaps if d is large enough, but it is very easy to verify that radiation reflected from a strip will be restricted to escape into the sky through the gap that beam radiation enters and three adjacent gaps as shown in Fig. 15 if d is less than $1.5D_2$ (this will absolutely ensure Δx, calculated by Eq. 63, less B). In practical applications, d is in range of $0.5D_2$–$1.5D_2$, and in this case, F_{w-T} can be simply calculated by:

$$F_{w-T} = 1 - \mathrm{F}_1 - \mathrm{F}_2 - \mathrm{F}_3 - \mathrm{F}_4 \tag{60}$$

where F_1, F_2, F_3, and F_4 are the shape factors from the irradiated strip to gaps 1, 2, 3, and 4, respectively, as shown in Fig. 15. Based on the definition of two-dimensional shape factor, one has

$$F_1 = \frac{\int_0^w (\sin \theta_2 - \sin \theta_1) dy}{2w} \tag{61}$$

y is the coordinate of any point at the irradiated strip measuring from the right edge, θ_2 and θ_1 are the angle of two rays emitting from y and tangent to the left and right tubes of the gap 1 relative to the normal of collector surface, respectively (see Fig. 15), and determined by following expressions [17]

$$\tan \theta_2 = \frac{-A_2 C + \sqrt{A_2{}^2 C^2 - \left(1 - A_2{}^2\right)\left(1 - C^2\right)}}{1 - C^2} \tag{62a}$$

$$\tan \theta_1 = \frac{A_1 C + \sqrt{A_1{}^2 C^2 - \left(A_1{}^2 - 1\right)\left(C^2 - 1\right)}}{\left(C^2 - 1\right)} \tag{62b}$$

where $A_2 = \frac{2(B+\Delta x-y)}{D_2}$; $A_1 = \frac{2(\Delta x-y)}{D_2}$; $C = \frac{2d}{D_2}$; Δx is the distance from the right edge of the irradiated strip to central line of the tube (see Fig. 15), and calculated by:

$$\Delta x = d\tan\Omega - \frac{D_2}{2\cos\Omega} \tag{63}$$

Similarly

$$F_2 = \frac{\int_0^{y_1}(\sin\theta_2 - \sin\theta_1)dy}{2w} \tag{64}$$

Where $y_1 = \min(w, \Delta)$, and $\Delta = \Delta x + d\tan\Omega_2 - 0.5B$. If $y_1 \le 0$, F_2 is taken to be zero. θ_2 and θ_1 in Eq. 64 are determined by Eqs. 62a and 62b but in this case $A_2 = \frac{2(B-\Delta x+y)}{D_2}$ and $A_1 = \frac{2(y-\Delta x)}{D_2}$. Similarly, we have

$$F_3 = \frac{\int_{y_2}^{w}(\sin\theta_2 - \sin\theta_1)dy}{2w} \tag{65}$$

where $y_2 = 1.5B + \Delta x - d\tan\Omega_2$, if $y_2 \le 0$, then y_2 is set at zero. If $y_2 \ge w$, F_3 is taken to be zero. θ_2 and θ_1 in Eq. 65 are also determined by Eqs. 62a and 62b, and in this case $A_2 = \frac{2(2B+\Delta x-y)}{D_2}$ and $A_1 = \frac{2(B+\Delta x-y)}{D_2}$.

F_4 in Eq. 59 is given by

$$F_4 = \frac{\int_0^{y_3}(\sin\theta_2 - \sin\theta_1)dy}{2w} \tag{66}$$

Where $y_3 = \min(w, \Delta_1)$, and $\Delta_1 = \Delta x + d\tan\Omega_2 - 1.5B$. If $y_3 \le 0$, F_3 is taken to be zero. θ_2 and θ_1 in Eq. 66 are determined by Eqs. 62a and 62b, but in this case $A_2 = \frac{2(2B-\Delta x+y)}{D_2}$ and $A_1 = \frac{2(B-\Delta x+y)}{D_2}$.

Given B, d, and Ω, the shape factor, F_{w_T}, can be obtained by numerical integration based on Eqs. 61, 62a, 62b, 63, 64, 65, and 66 as shown in Fig. 16.

Radiation Reflected from the DFR Due to the Irradiation of Sky Diffuse Radiation Through Gaps Between Solar Tubes

Radiation reflected from DFR irradiated by sky diffuse radiation through gaps is calculated by integrating Eq. 56 over the projection angle, Ω, of solar ray. For T-type collectors, this can be done by:

$$\begin{aligned} I_{dr} &= \frac{D_1}{D_2}\int_{-\Omega_2}^{\Omega_2} i\cos\Omega w\rho F_{w-T}d\Omega = \frac{D_1 I_{d\beta}\rho}{D_2}\int_0^{\Omega_2} wF_{w-T}\cos\Omega d\Omega \\ &= \pi D_1 I_{d\beta}\rho F_{d-T} \end{aligned} \tag{67}$$

where $F_{d-T} = \frac{1}{\pi D_2}\int_0^{\Omega_2} wF_{w-T}\cos\Omega d\Omega = F_0$ is termed as the shape factor from DFR to tubes for sky diffuse radiation, $I_{d\beta} = 0.5(1 + \cos\beta)I_d$. Similarly, for H-type collectors, I_{dr} is determined by

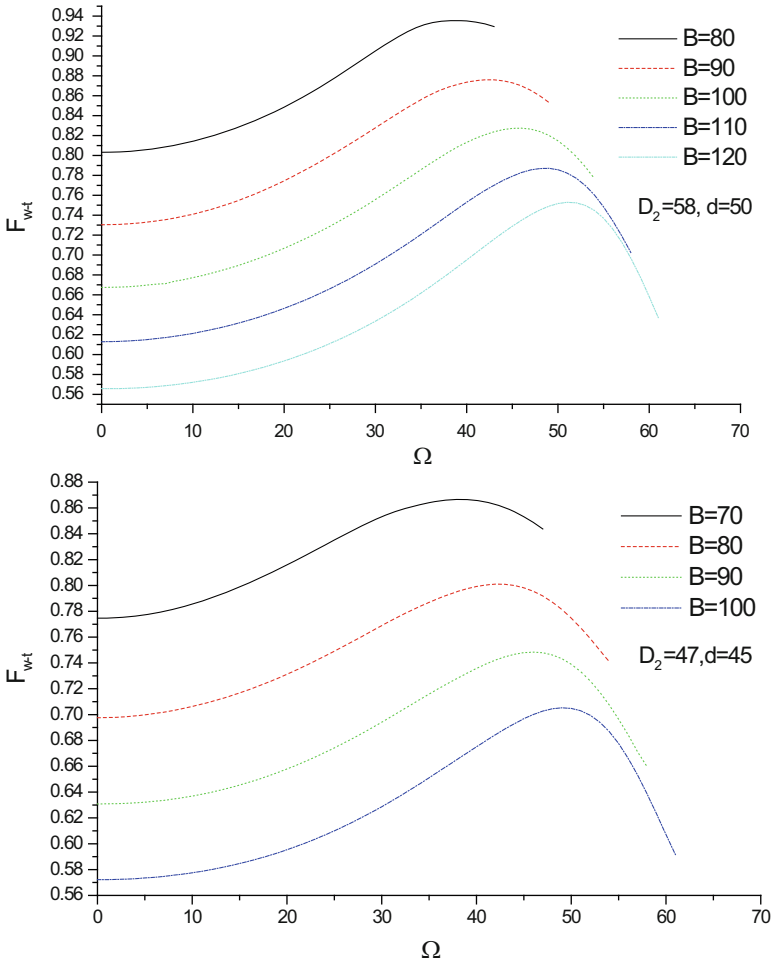

Fig. 16 Variation of shape factor F_{w-t} with Ω for solar tube collector with DFR

$$I_{dr} = \frac{D_1}{D_2}\int_{-\Omega_x}^{\Omega_2} i\cos\Omega w\rho F_{w-T}d\Omega = \frac{D_1 I_d \rho}{2D_2}\left(\int_0^{\Omega_2} wF_{w-T}\cos\Omega d\Omega + \int_0^{\Omega_x} wF_{w-T}\cos\Omega d\Omega\right) = \pi D_1 I_d \rho F_{d-T} \tag{68}$$

where

$$F_{d-T} = \frac{1}{2\pi D_2}\left(\int_0^{\Omega_2} wF_{w-T}\cos\Omega d\Omega + \int_0^{\Omega_x} wF_{w-T}\cos\Omega d\Omega\right) = 0.5F_0(1+K(\Omega_x)) \tag{69}$$

where

$$\Omega_x = \min(0.5\pi - \beta, \Omega_2) \tag{70a}$$

$$K(\Omega_x) = \frac{1}{\pi F_0 D_2} \int_0^{\Omega_x} wF_{w-T} \cos\Omega d\Omega \tag{70b}$$

Given the geometry of collectors, F_0 is a constant, but $K(\Omega_x)$ is dependent on the tilt-angle of H-type collectors. Both of F_0 and $K(\Omega_x)$ must be obtained by numerical calculations.

Radiation at any moment collected by unit length of a single tube of a collector can be calculated by summing all four components mentioned above as follows:

$$I_t = D_1\left(I_b \cos\theta_t f(\Omega) + \pi I_{d\beta} F_{T-S} + I_b \cos\theta_c \rho w F_{w-T}/D_2 + \pi I_{d\beta}\rho F_{d-T}\right) \tag{71}$$

Daily collectible radiation on unit length of a tube, H_{day}, can be calculated by integrating I_t in Eq. 71 over the daytime:

$$H_{day} = D_1 \int_{-t_s}^{t_s} I_b(\cos\theta_t f(\Omega) + \cos\theta_c \rho w F_{w-T}/D_2)dt + \pi D_1(F_{T-s} + \rho F_{d-T})H_{d\beta} \tag{72}$$

For T-type collectors, $H_{d\beta} = 0.5(1 + \cos\beta)H_d$; whereas for H-type collectors, $H_{d\beta} = H_d$, and H_d is the daily diffuse radiation on the horizon. t_s in Eq. 72 is the sunset time on the horizon measured from the solar noon. Therefore, given the time variation of I_b and H_d in a day, the daily radiation collected by unit length of a tube can be numerically obtained, the summing daily collectible radiation in all days of a year obtains annual collectible radiation on unit length of a single tube ($S_{a,\,t}$), and annual radiation collected by unit area of solar tube collector is given by:

$$S_{a,c} = \frac{NS_{a,t}}{(N-1)B + D_2} \tag{73}$$

In solar calculations, monthly horizontal radiation averaged over many years was widely used, and monthly average daily sky diffuse radiation on the horizon (H_d) and the time variation of I_b in a day are estimated based on the correlations proposed by Collares-Pereira and Rabl [18].

Optical Performance of Solar Tube Collectors

The most common ET in the market are ones with $D_2 = 58$ mm and $D_1 = 47$ mm, and ones with $D_2 = 47$ mm and $D_1 = 37$ mm tubes. Thus, optical performance analysis is performed here based on the tubes measuring 47/58 and 37/47 in diameter of inner tube/cover tube.

Effects of Distance from Center of Tubes to DFR on the Annual Collectible Radiation

Figure 17 indicates that, with the increase in d, the annual collectible radiation on unit length of a single tube increases generally, but such increase becomes slow and comes to a halt when d is larger than $1.2D_2$ for collectors with $D_2 = 58$ and $B = 80$, and $1.4D_2$ for collectors with $D_2 = 58$ and $B = 100$. In practical applications, setting d to be in the range of (1–1.2) D_2 is advisable.

Effects of Distance Between Tubes on the Annual Collectible Radiation

Figure 18 shows effects of central distance between tubes on the annual collectible radiation. Obviously, the annual collectible radiation on unit length of a single tube, $S_{a,\ t}$, increases with the increase of B especially for collectors with DFR, but the annual collectible radiation on unit area of solar collector, $S_{a,\ c}$, decreases. In most application, B is about 80 mm for solar tubes of 47/58 and 70 mm for those of 37/47.

Optimal Tilt Angle of South-Facing Collectors

As shown in Tables 1 and 2, for a specific site, the optimal tilt-angle of south-facing solar tube arrays for maximizing annual collectible radiation on unit length of a single tube is dependent on the type and structure of tube arrays. In general, the optimal tilt-angle is less than the site latitude, the optimal tilt-angle of T-type collectors, $\beta_{T,\ opt}$, is larger than that of H-type collectors, $\beta_{H,\ opt}$, and optimal tilt-angle decreases with the increase in B for a given collector type, especially for H-type collectors. For H-type collectors, the use of DFR makes the optimal tilt-angle increase greatly. For areas with abundant solar resources, such as Lhasa, the optimal tile-angle of H-type collectors is close to the site latitude, whereas for the areas with poor solar resources, such as Chengdu, the optimal tilt-angle is much less than the

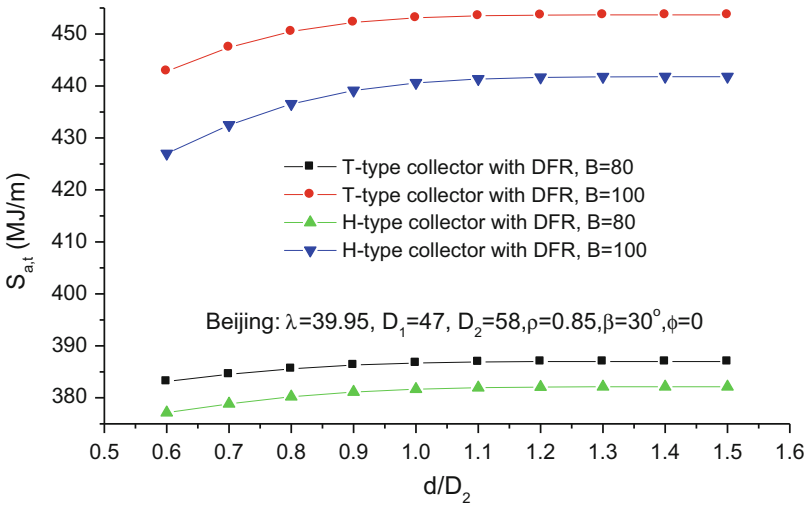

Fig. 17 Effect of distance of tubes from the DFR (From Tang et al. [17])

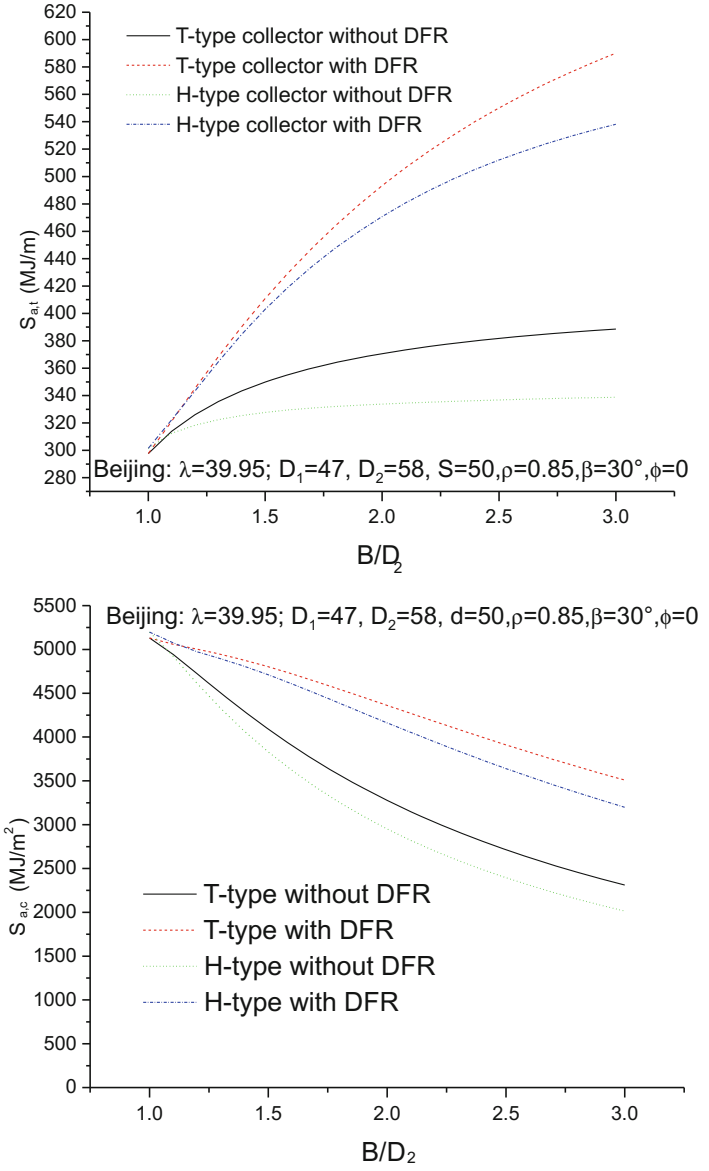

Fig. 18 Effects of space between tubes on the annual collectible radiation (From Tang [17])

site latitude. For most areas with site latitude larger than 30°, the optimal tilt-angle of T-type collectors is 10° less than the site latitude, and that of H-type collectors without DFR is about 20° less than site latitude. Unlike flat-plate collectors, which have the optimal tilt-angle close to the site latitude [19], all-glass evacuated tube collectors should be tilted at angle less than the site latitude in order to collect more

Table 1 Optimal tilt-angle of collectors without DFR ($D_1 = 47$, $D_2 = 58$) (From Tang [17])

Location (site latitude)	B = 80		B = 90		B = 100	
	$\beta_{T,\,opt}$	$\beta_{H,\,opt}$	$\beta_{T,\,opt}$	$\beta_{H,\,opt}$	$\beta_{T,\,opt}$	$\beta_{H,\,opt}$
Beijing (39.95°)	30.5	17.2	29.8	13.9	29.3	11.5
Harbin (45.75°)	34.8	21.3	34	17.3	33.4	14.5
Urumqi (43.78°)	31.6	19.4	30.9	15.5	30.3	12.9
Lanzhou (36.02°)	26.9	14.6	26.4	11.7	25.9	9.6
Xi'an (34.25°)	21.9	11.9	21.4	9.2	20.9	7.5
Shanghai (31.2°)	20.2	10.3	19.7	8	19.3	6.5
Chengdu (30.67°)	15.4	8.2	14.9	6.2	14.5	5
Lhasa (29.72°)	26.5	13.9	26.1	11.4	25.8	9.6
Kunming (25.01°)	21	10.1	20.7	8.1	20.3	6.9
Guangzhou (23°)	15.4	7.5	15.1	6	14.8	5

Table 2 Optimal tilt-angle of collectors with DFR ($D_1 = 47$, $D_2 = 58$, $S = 50$,$\rho = 0.85$) (From Tang [17])

Location (site latitude)	B = 80		B = 90		B = 100	
	$\beta_{T,\,opt}$	$\beta_{H,\,opt}$	$\beta_{T,\,opt}$	$\beta_{H,\,opt}$	$\beta_{T,\,opt}$	$\beta_{H,\,opt}$
Beijing (39.95°)	31.6	28.6	31.4	26.8	31.1	24.8
Harbin (45.75°)	36.1	32.6	35.8	30.7	35.6	28.5
Urumqi (43.78°)	32.8	30.2	32.6	28.5	32.4	26.5
Lanzhou (36.02°)	27.9	25.5	27.7	23.8	27.5	21.9
Xi'an (34.25°)	23	21.2	22.8	19.8	22.6	18.1
Shanghai (31.2°)	21.2	19.5	21	18	20.9	16.3
Chengdu (30.67°)	16.5	15.5	16.3	14.4	16.2	12.9
Lhasa (29.72°)	27.1	24.6	27	23.2	26.9	21.4
Kunming (25.01°)	21.6	19.3	21.5	17.8	21.4	16.1
Guangzhou (23°)	16.3	14.9	16	13.6	15.9	12.2

sky diffuse radiation, especially in the areas with poor solar resources. The study by Tang et al. [17] showed that T-type collector annually collects about 5% more radiation compared to H-type collector, for most areas in China, setting the tilt-angle of south-faced T-type collector at the site latitude is acceptable, but for H-type collectors without DFR it is not reasonable.

Comparison of Annual Collectible Radiation Between Flat-Plate and Evacuated Tube Collectors

Theoretically, the evacuated solar tube just like a single axis sun-tracked solar panel is more efficient for radiation collection than flat-plate collector. But for solar tube collectors, solar tubes would shade each other. Furthermore, a fraction of incident radiation would not be intercepted by tubes due to gaps between tubes; therefore, radiation received by unit area of solar tube array might be less than that of flat-plate collector. Table 3 presents the ratio of radiation yearly collected by unit area of flat-plate collector to that by unit area of solar tube collector used in Kunming of

Table 3 Ratio of annual radiation collected by flat-plate collector to that by solar tube collectors in Kunming of China ($\varphi = 0$, $D_1 = 48$ mm, $D_2 = 58$ mm, B = 70 mm, d = 50 mm, $\rho = 0.8$)

	Without DFR		With DFR	
β	T-type collector	H-type collector	T-type collector	H-type collector
20	1.306	1.339	1.234	1.243
5	1.306	1.346	1.234	1.245
40	1.304	1.345	1.233	1.244
0	1.298	1.32	1.231	1.234
90	1.286	1.24	1.232	1.213

China. Results show that flat-plate collector annually receives about 20% and 30% more radiation compared to solar tube collectors with and without DFR, respectively. This means that flat-plate collector may be more attractive in the areas where freezing temperature does not occur in the winter.

Solar Hot Water Systems

Classification of Solar Water Systems

A solar hot water system usually consists of collectors, water storage tank, pipes, pump, auxiliary heater, etc. arranged in different ways. As shown in Fig. 19, solar water heating systems can be classified according to the driven force for circulation of heat transfer fluid in the system as:

- Natural circulation (also termed as passive system)
- Forced circulation
- One-through system
- In practical applications, the one-through solar system, where the hot water from collectors is directly drained to the hot water storage tank when the temperature of water in collectors reaches the desired value, is rarely found due to the unsteady hot water supply to load. Based on whether the antifreeze loop is used in solar water systems, solar water systems are divided into:
- Direct system
- Indirect system

Therefore, solar water systems shown in Fig. 19 are direct system, and those shown in Fig. 20 are indirect system. In the area where freezing temperatures occur in winters, antifreeze of solar collectors must be considered, and one of the methods is to use antifreeze heat transfer fluid in solar collector. The collector heat exchangers can be either internal or external to the water tank; however, such system would suffer penalty in its thermal performance resulting from the use of heat exchanger. In practical applications, the antifreeze of solar collectors can be achieved by other passive and active ways according to the local climatic conditions and characteristics

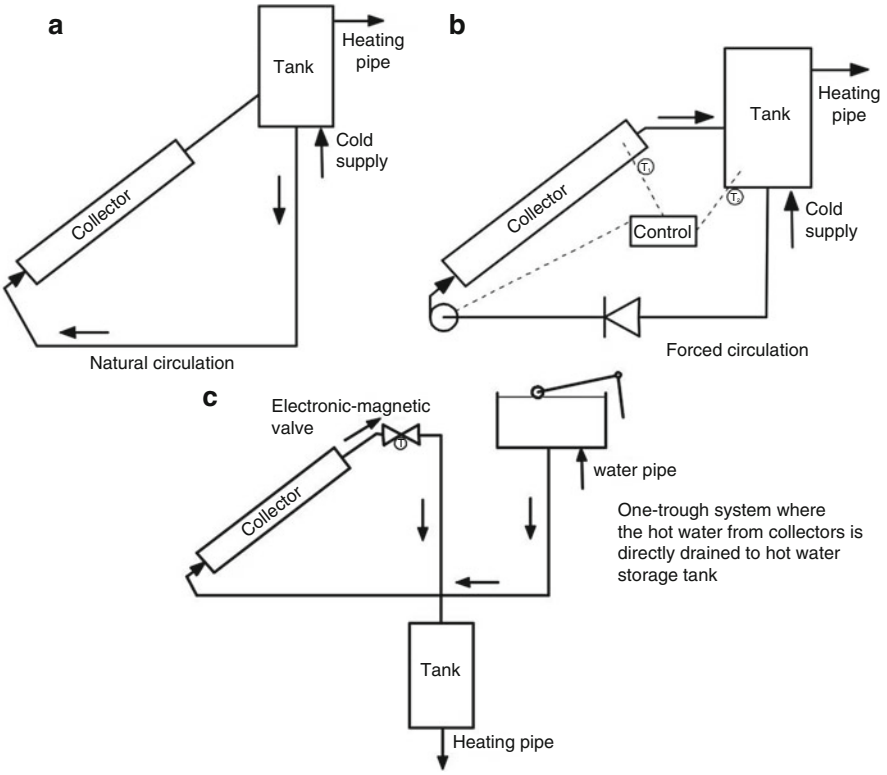

Fig. 19 Scheme of natural circulation, forced circulation, and one-trough solar systems. (**a**) Natural circulation, (**b**) forced circulation, and (**c**) one-trough system, where the hot water from collectors is directly drained to hot water storage tank

of solar water system in the structure [20, 21]. For domestic solar water heaters used in areas with warm winters, the reverse flow at night is an effective and simple way for antifreeze as aforementioned [22]. Whereas for forced circulation solar water system, antifreeze can be simply implemented by turning on the pump (which is used to circulation the system in the day) to circulate the hot water in the hot storage tank as the water temperature inside the collectors close to freezing point.

According to modes of hot water supply in buildings, solar water systems are categorized as

- Individual hot water supply system
- Collective water supply system
- Collective-individual hot water supply system

As shown in Fig. 21a, one system only provides hot water to one user or family, and sometimes such system is termed as domestic solar water heater. For solar system shown in Fig. 20b, users or families share hot water from a storage tank in

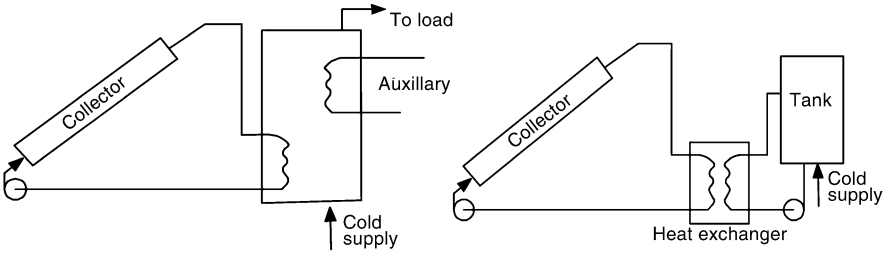

Fig. 20 Indirect solar water systems

Fig. 21 (**a**) Domestic solar water heaters, (**b**) collective solar hot water supply system, (**c**) collective-individual hot water supply system

a solar water system; such systems are commonly employed in the dormitory of schools, hotels, hospital, public bathhouse, and even residential buildings. The collective hot water systems share the advantages of high thermal efficiency due to less heat loss from water storage tank and pipes, low cost and flexible hot water supply for all users those can use hot water as actually required. In high residential buildings, the hot water demand is high but roof area for the installation of solar

collectors is limited; thus, to provide sufficient hot water for all users as possible, all of rooftop is equipped with solar collectors, as shown in Fig. 21c, and the hot water from solar collector arrays on the rooftop and southern elevation of a high building is directly distributed to water storage tanks located in each house of the building then returned to collectors for circulation.

Passive Solar Water Heaters

Solar Water Heaters with Flat-Plate Collectors

Natural circulation system is a simplest solar system. In such system, the water tank is located above the solar collectors. When the water in collectors gains solar heat and becomes light, it moves along pipes of flat-plate collectors or upper wall of evacuated solar tubes to the tank driven by the buoyancy force; thus, the thermosiphonic circulation is formed in the tank-collector loop. The driven force of the natural circulation is dependent on the water temperature distribution along the thermosiphonic circulation loop. As shown in Fig. 22, assuming the distribution of water temperature in the tank and collector along the water flow direction is linear, and both pipes connecting collector and tank are thermally insulated, the hydraulic head for water circulation can be simply estimated by:

$$\begin{aligned} h_{th} &= \rho_m g h_1 + \rho_1 g h_2 + \rho_1 g h_3 - \rho_2 g h_1 - \rho_2 g h_2 - \rho_m g h_3 \\ &= (\rho_1 - \rho_2) g h_2 + (\rho_1 - \rho_m) g h_3 + (\rho_m - \rho_2) g h_1 \end{aligned} \tag{74}$$

where $g = 9.8$ m/s^2 is the gravity acceleration, the ρ_1, ρ_2, and ρ_m are the density of water corresponding to temperature T_1, T_2, and T_m (equal to $0.5(T_1 + T_2)$ for linear water distribution), respectively. During the daytimes, $T_2 > T_m > T_1$, thus $\rho_1 > \rho_m > \rho_2$, and the larger the height of storage tank above the top of collectors (h_2), the larger the thermosiphonic force (h_{th}). Equation 74 also indicates that vertical

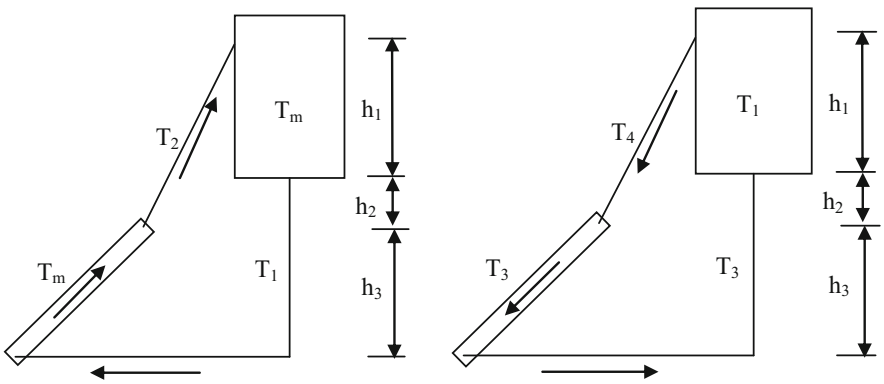

Fig. 22 *Left*: Temperature distribution of water in natural solar system in the daytime; *right*: temperature distribution of water in natural solar system at night

cylindrical tanks facilitate water circulation compared to horizontal cylindrical tanks. On the other hand, the hydraulic loss due to friction of water flow along the circulation loop is a quadratic function of water mass flow rate ($\dot{m}$) [23–25] as:

$$h_f = A\dot{m} + B\dot{m}^2 \tag{75}$$

where constants A and B are dependent on configuration of the circulation loop. It is known from Eq. 74 that the water flow rate would increase with the temperature difference across solar collector (i.e., $T_2 - T_1$), and in turn, it results in the decrease in temperature difference. Equation 75 also indicates that high mass flow rate results in high hydraulic loss, and in turn, it results in the decrease in flow rate. This means that natural solar systems are capable of self-adjusting for operation. The early work done by Close [26] showed that the temperature rise of water flowing through collectors was about 10 °C, and water circulated through the collector several times a day.

At night, especially clear nights, the temperature of water in collectors would decrease due to heat loss to the ambient air especially thermal radiation from the absorber to the sky dome, then water in collectors moves down after being cooled, and the reverse flow is formed, leading more heat lost. As shown in Fig. 22 (right), it is assumed that the temperature of water in the collector and the down connecting pipe is identical; thus, the hydraulic head for reverse flow is estimated by:

$$h_{th} = (\rho_4 - \rho_1)gh_1 + (\rho_4 - \rho_3)gh_2 \tag{76}$$

The first term in the right side of Eq. 76 is positive due to $T_4 < T_1$ thus a driven force for reverse flow, and the second term is negative due to $T_4 > T_3$ thus a force to resist reverse flow. This means that increasing the height difference between the bottom of tank and top of collectors facilitates the reduction of heat loss resulting from reverse flow at night, and the use of vertical cylindrical tank would assist in reverse flow.

Experimental measurement by Tang et al. [5] showed temperature of water stagnant in collectors at clear nights was about 7 °C lower than ambient air temperature, and that of water in collectors was close even slightly higher than the ambient air temperature if the reverse flow was allowed. This means that reverse flow in the natural circulation system is a double-edged weapon; on the one hand, reverse flow results in more heat loss at night, but on the other hand, it facilitates antifreezing of collectors when the air temperature is close to freezing point [5, 22].

Solar Water Heaters with Evacuated Tubes

Passive solar water heaters with evacuated tubes include water-in-glass solar water heater and the one with separate solar tube arrays as shown in Fig. 21a, b. Recent report shows that water-in-glass evacuated tube solar water heaters are common and take about 90% share of domestic solar water heater market in China, whereas natural circulation solar water systems with separate solar tube arrays are common in the collective solar water supply system.

As shown in Fig. 23, when the incident solar radiation is absorbed by the inner tube, the water heated by the wall of tubes would move along the upper wall to tank/header, meanwhile, the cold water from tank/header flows along the lower wall to the sealed end of tubes. Visualizing experiment in laboratory by Huo et al. [27] showed that, for south-north oriented solar tubes inclined at a tilt-angle from the horizon, a fraction of cold water from the water tank on the way circulating down to the sealed end would return back to the tank and never reach the sealed end; furthermore, such fraction increased with the increase in the tilt-angle. Outdoor experimental results by Tang et al. [28] showed that the water temperature difference between outlet and inlet at the opening end of tubes was kept at 1–2 °C. For the water-in-glass solar water heaters tilted at 22° from the horizon, a clear water circulation as shown in Fig. 23a was found, whereas for solar heater tilted at 46°, the situation in the morning was the same as that tilted at 22°, but in the afternoon, the cold water from the storage tank on the way to the sealed end was partially or fully mixed with the hot water returning to the storage tank without a clear water circulation loop as shown in

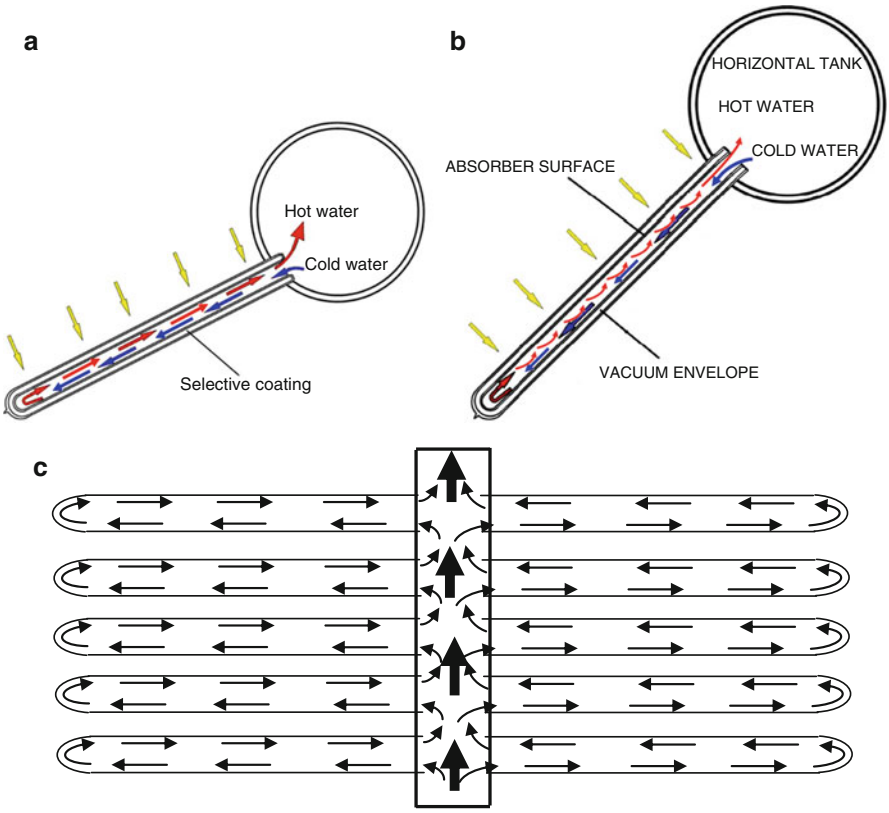

Fig. 23 Scheme of water flow in solar tubes (**a**) water-in-glass solar water heater tilted at lower angle, (**b**) water-in-glass solar water heater tilted at the angle larger than 45 °C, (**c**) solar water heater with a horizontally oriented tube array

Fig. 23b. Furthermore, such mixing became more intense with the increase in water temperature in the tank. These studies imply that the increase in the tilt angle of water-in-glass evacuated tube solar water heaters has no positive effect on their thermal performance, and in turn, it results in inactive region near the sealed end of tubes. Studies by Tang [28] and Yang [29] showed that, with the increase of space between two adjacent tubes for water-in-glass solar heaters, the daily solar heat gain of a single tube increases but the daily solar heat gain per unit area of collectors decreases. Recent experimental results of Tang et al. [30] revealed that reverse flow inside tubes at night was observed but the heat loss resulting from reverse flow was insignificant.

For passive solar water heater with a separate solar tube array, the evacuated solar tubes are horizontally oriented, the driven force for thermosiphonic circulation originates from the temperature difference of water in header of solar tube arrays, and the water tank is located above the solar tube arrays. As shown in Fig. 23c, when solar tubes are irradiated by incident radiation, the heated water flows out of tubes along the upper wall of tubes, meanwhile the cold water flows in tube along the lower wall of tubes, and a thermosiphone circulation loop is formed in the system. A numerical study by Shah and Furbo [31] indicated that the shorter tube generally achieved the higher heat transfer efficiency from tubes to the header, and the best flow velocity in header is 0.4–1 m/min for forced circulation system because higher velocity of water in header would lead to "short circuit of flow." To facilitate heat transfer from tubes to the header, 3–5° tilt-angle of tubes from the horizon is advisable.

Forced Circulation System

Passive solar systems share the advantages of simple in structure, less maintenance, reliability in operation, and high performance. However, such system is only suitable for small-scale solar system due to small thermosiphonic hydraulic head for the circulation, and for a large-scale solar water system, a pump should be used for water circulation as shown in Fig. 19b. In general, two types of control strategies are used in forced circulation solar systems: on-off and proportional. With an on-off controller, a decision is made to turn the circulating pump on or off depending on whether or not useful output hot water is available from collectors. With a proportional controller, the pump speed is varied in such way to maintain a specified temperature level at the outlet of collectors. The choice of control strategies is largely determined based on the ultimate use of collected energy.

For a solar water system equipped with an on-off controller, two temperature sensors are commonly used: one in the bottom of storage and one in the absorber plate at the exit of a collector or on the pipe near the exit of collector. When water is flowing, the sensor near the exit of collectors senses the exit water temperature and the sensor at the bottom measures the inlet water temperature (T_i), whereas when water is not flowing, the sensor measures the temperature of water in collectors. Whenever the water temperature in collectors at no-flow conditions exceeds T_i by a

specific amount (ΔT_{on}), the controller sends a signal to turn on the pump, and to turn off the pump as the temperature difference between outlet and inlet of collectors is less than a specific amount ΔT_{ff}. One must note that the mass flow rate of water circulation would affect daily average thermal conversion efficiency to some extent, and high mass flow rate would deteriorate temperature stratification in the tank, resulting in the reduction of daily efficiency of the system. The reasonable mass flow rate of pumps is that to ensure the water in tanks circulating 2–3 times a day, or 30–50 g/s for unit area of solar collectors.

Orientation of Solar Collectors

To maximize annual radiation collection of solar collectors, solar panels are usually oriented towards the equator with an optimal tilt-angle from the horizon. In general, the optimal tilt-angle of a collector is related to local climatic conditions, site latitude, and period of its use [19]. For yearly fixed flat-plate south-facing solar collectors, the optimal tilt-angle, dependent on local climatic conditions and site latitude, is usually about the site latitude, and 10° of deviation from the site latitude and 20° of azimuth angle from due south result in the reduction of annual radiation collection less than 5% [17]. Thus, for yearly fixed flat-plate collectors, the reasonable orientation should be $\beta = \lambda \pm 10^\circ$ and $\varphi = \pm 20^\circ$. For solar collectors with azimuth angle larger than 30°, the tilt-angle should appropriately decrease in order to increase daily sunshine hours of collectors (Fig. 24).

Distance Between Collectors

In large-scale solar systems, a number of solar collectors are required and they might be arranged in many rows. As shown in Fig. 25, all collectors in the collector array are oriented φ west from due south, and to avoid shadow of collectors falling on those behind at a given moment in day, the least distance of collectors between two rows should be subjected to:

$$D = H \tan \theta_{xoz} = -\left(n_y \sin \varphi + n_z \cos \varphi\right)/n_x \tag{77}$$

For south-faced solar collectors, the Eq. 76 is simplified as:

$$D/H = \frac{-n_z}{n_x} = \frac{\cos \delta \sin \lambda \cos \omega - \sin \delta \cos \lambda}{\cos \delta \cos \lambda \cos \omega + \sin \delta \sin \lambda} \tag{78}$$

It is known from above that, given ω and λ, the least distance depends on δ and reaches the maximum on the winter solstice ($\delta = -23.45^\circ$); thus, for yearly fixed solar collectors, the least distance of collectors between two rows can be determined based on the Eq. 76 by setting $\delta = -23.45^\circ$ and the hour angle (ω) at the moment all

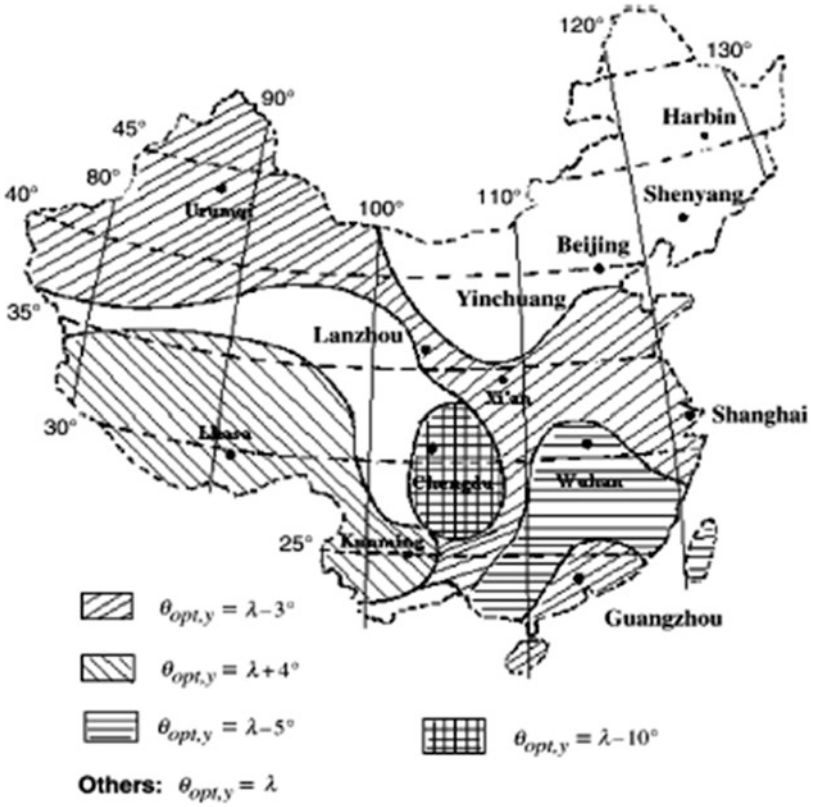

Fig. 24 Optimal tilt-angle of south-facing solar collector used in China (From Tang and Wu [19])

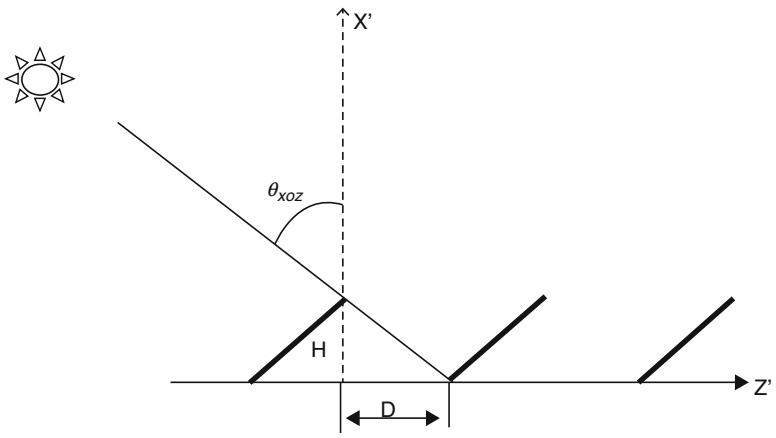

Fig. 25 The least distance of collectors between two rows

collectors are required to fully be irradiated by the sun. For example, all collectors are required to be fully irradiated by the sun at the solar noon in all days of a year, the least distance is as:

$$R = D/H = \cos\varphi \tan(\lambda + 23.45) \tag{79}$$

And for south-faced solar collectors, it becomes:

$$R_s = D/H = \tan(\lambda + 23.45) \tag{80}$$

The analysis by Tang et al. [32] shows that, in a collector array, the distance (D) between two adjacent rows of collectors has a significant effect on the annual collectible radiation on the collectors (S_2) in the second row compared with those in the first row (S_1), and such effect becomes small as D/H is close to R_s. It is also found that, for south-faced collectors in the case of D/H = R_s, S_s/S_1 is higher than 0.95 in all sites over China, thus, setting D/H = (0.9–1) × tan(λ + 23.45) is advisable in practical applications (Fig. 26).

Arrangement of Solar Collectors

Flow Distribution in Collectors

In order to make the thermal performance of all collectors identical, it is essential to ensure flow rate of water through all collectors is identical in a collector array. Therefore, the arrangement of solar collectors is important in obtaining good thermal performance in the design of solar water systems. It is particularly significant in larger scale forced-circulation systems; natural circulation systems tend to be self-adjusting, and thus nonuniform flow distribution is not as critical. The earlier work of Dunkle and Davey [33] showed that the pressure drop of water flowing across a riser of a collector from the bottom header to the top header differs for different riser (see Fig. 27). The implications of these pressure distributions are obvious: the pressure drops of water flowing through risers at ends are greater than risers near the center, leading lower water temperature in the end riser due to high flows and higher water temperature in the center risers due to low flows.

Experimental measurements by Dunkle and Davey [33] found that the absorber temperature in collectors near the center in a string of 12 collectors connected in parallel are much higher than collectors at ends as shown in Fig. 28. This implies that the collectors at ends perform better than collectors at the center, especially for high flow rate, and the number of collectors connected in parallel in a row is not allowed to be too greater in order to make solar systems perform well, and a maximum of 8–12 collectors connected in parallel is recommended. These results also show that high flow rate in the forced-circulation solar systems is not advisable, and the pumps should be appropriately selected based on requirements of water flow rate, for example, making the water in the storage tank circulate 1.5–2.5 times during 8 h of operation.

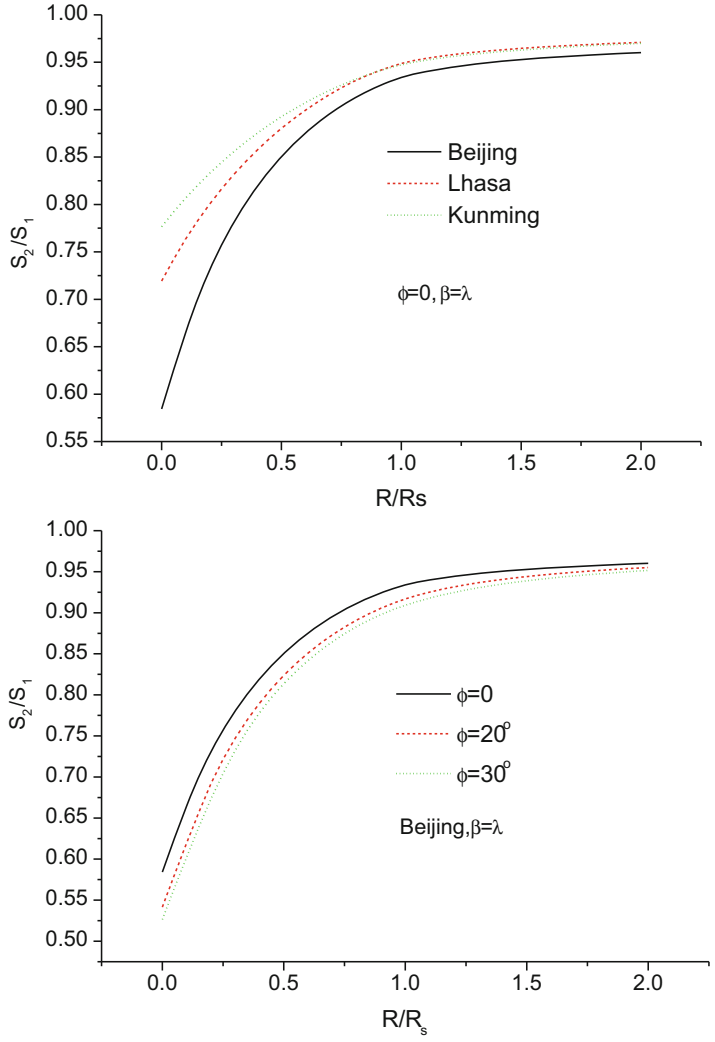

Fig. 26 Effects of D/H on the annual collectible radiation on collectors compared with those in the first row in a collector array (From Tang [32])

Arrangement of Collectors

In the design of arrangement of solar collectors and connecting pipes, the basic requirement is to ensure flow rate of water through all collectors identical as possible. The implication of this requirement is that the path length of all water loops flowing through all collectors and connecting pipes during the water circulation should be identical as possible. Basic collector arrangements include parallel, series, and parallel-series. Figure 29 presents possible collectors' arrangements. From the point view of the flow distribution, Z-type and parallel-series arrangements are advisable and C-type

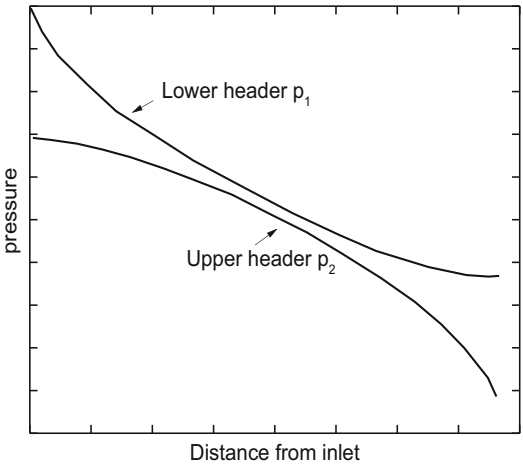

Fig. 27 Pressure distribution in headers of a collector (From Dunkle and Davey [33])

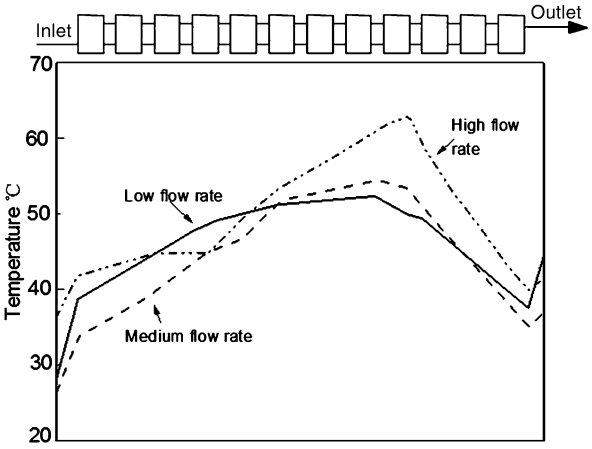

Fig. 28 Measured temperature on the plates in a string of 12 collectors connected in parallel (Dunkle and Davey [33])

arrangement is not reasonable especially for large-scale forced-circulation systems due to the presence of "short-circuit of water flow" during the water circulation. Similarly, the arrangement of collecting pipes is also important to ensure uniform flow rate through all collectors. Figure 30 shows a typical arrangement of connecting pipes in a natural circulation solar system with Z-type collector arrangement of multiple-parallel.

Application of Solar Water Systems in Buildings

Specially Designed Solar Collectors as Roof Material of Buildings

Although solar water systems have got wide use in buildings over the world, works on the building integration of solar energy systems just began, those done in the past are simply to integrate solar water heating systems into buildings based on the purely aesthetic

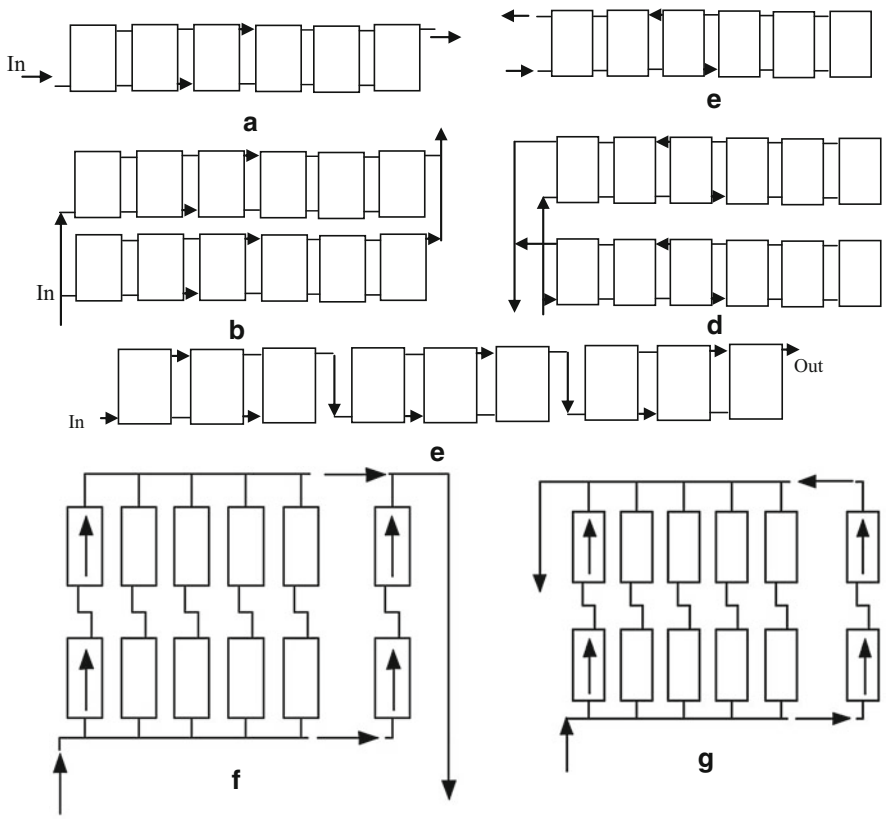

Fig. 29 Methods of connecting collectors in (**a**) parallel with inlet and outlet at two ends (Z-type arrangement), (**b**) parallel arrangement with inlet and outlet at the same end (C-type arrangement), (**c**) Z-type arrangement of multiple-parallel, (**d**) C-type arrangement of multiple-parallel, (**e**) parallel-series arrangement, (**f**) Z-type arrangement of series-parallel, and (**g**) C-type arrangement of series-parallel

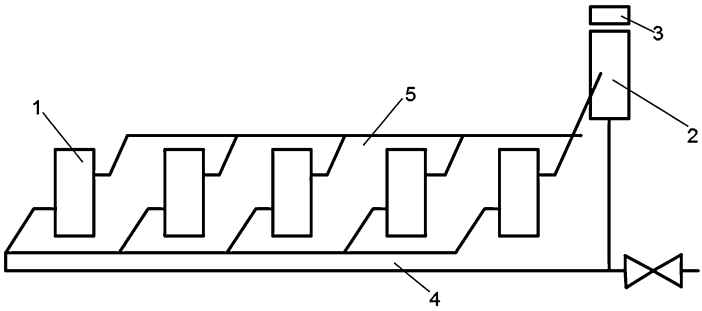

Fig. 30 A typical arrangement of connecting pipes and collectors. (*1*) String of collectors connecting in parallel, (*2*) hot water tank, (*3*) tank for cold water supply, (*4*) pipe for distributing cold water to collectors, (*5*) pipe for collecting hot water from collectors

requirements in a building, and far away from the true "solar buildings or energy-efficient buildings." It is in recent years that the idea of building integration of solar energy systems is well understood by architects due to the appeal of energy-efficient buildings from governments. The basic requirement of so called "integration of solar systems with buildings" is that the planning, design, construction, and final examination of a building must be kept in the same step with those of solar systems, rather than performing the design and installation of solar water systems when the construction of the building is completely finished. A key issue to achieve building integration of solar energy systems is to make solar elements as parts of buildings. Thus, for a solar element as an alternative to building elements, it is required to have a similar or same lifetime, price, and function as a regular building element, and furthermore, it must be commercially available in the market and easy to maintain and replace. Unfortunately, solar collectors commercially available in the market cannot function as building elements.

Recently, a solar thermal module developed by Xinyuan Sunlight Scientific Co. Ltd. of Kunming, China, has got some practical applications. This solar thermal module, similar to the commonly used flat-plate collectors, consisted of an aluminum tube-fin absorber as shown in Fig. 31, has a fixed width (600 mm) but a flexible length which can be extended to 9 m based on the practical requirement. The back insulation of the module is 60 mm polystyrene panel sandwiched in between two colored iron sheets, and the cover is 1 mm polycarbonate sheet. Holes through the absorber and back insulation of the module are drilled for daylight when needed (Fig. 32). A noticeable feature of the module is that modules can be easily assembled together to form a facade of buildings.

Figure 33 shows an office building at Xinyuan Sunlight Scientific Co. Ltd. of Kunming. The three fourths of the south-facing roof is covered by 275 m^2 solar water heating modules that replace the traditional roofing materials, thereby eliminating the need of conventional roof materials. The remaining part of the south-facing roof is covered by polycarbonate sheet, and provides direct solar radiation for space heating of south-facing offices in winters. This system provides hot water to 60 workers dwelling in a nearby dormitory for the bath and heat for space heating of north-facing offices of the building. Holes on the solar modules provide the daylight to the offices underneath. Figures 34 and 35 show solar water collectors imbedded into roofs of residential buildings for hot water supply and space heating.

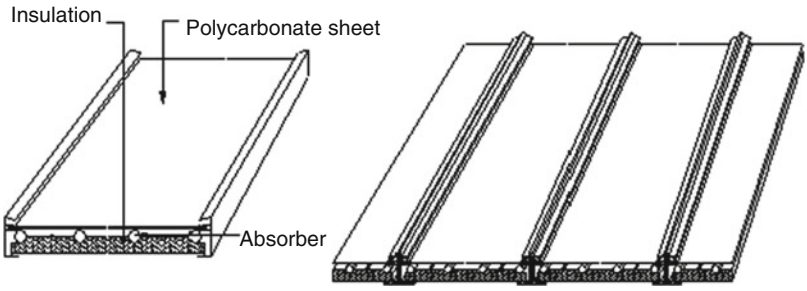

Fig. 31 A solar water collector module. *Left*: a single module; *right*: multi-module assembled together

Fig. 32 Solar water modules with perforated absorber for the daylight (Courtesy of Xinyuan Sunlight Co)

Fig. 33 *Left*: South-roof covered by solar water modules; *right*: holes on the solar collector modules provide daylight to the office (Courtesy of Xinyuan Sunlight Co)

Fig. 34 *Left*: South-roof partially covered by solar collectors. *Right*: Bedrooms heated by the solar water heating system (Courtesy of Xinyuan Sunlight Co)

Solar Collectors Integrated with Façade of Buildings

In recent years, solar elements as roofing materials integrated into buildings have been well understood and widely adopted by architects and solar designers due to many advantages, such as aesthetically compatible combination between solar

elements and buildings, and the cost reduction of the whole building due to the replacement of roofing materials by solar collector modules. However, such building integration of solar energy systems is restricted to low buildings with gable roofs. For high buildings, such building integration of solar systems is impossible to meet the demand of hot water for all households due to limited roof area for the installation of solar collectors, and solar elements integrated with the façade of buildings might be one of the potential solutions. The common methods include integrations of solar collectors with balconies and walls (Fig. 36). Figure 37 shows solar collectors as overhang shelter of windows, and Fig. 38 shows solar collectors as the sky light of living rooms.

Applications of Solar Water Heating System in High Buildings

In recent years, high residential buildings become common due to the shortage of lands available for building construction in cities, especially large cities. For high residential buildings, the roof area for the installation of solar water heating systems is limited and the capacity of occupants is high; thus, solar water heating systems on

Fig. 35 Solar collectors were imbedded into roofs of buildings in Kunming (Courtesy of Xinyuan Sunlight Co)

Fig. 36 Solar collectors integrated into balcony and walls of buildings (Courtesy of Xinyuna Sunlight Co)

Fig. 37 Solar collectors as the overhang shelter of windows

Fig. 38 Solar collectors as the sky-light of living rooms (Courtesy of Xinyuan Sunlight)

the roof is impossible to meet the requirement of hot water supply for all occupants. Therefore, fully utilizing roof and wall for the installation of solar collector is necessary. For meaningful applications, wherever solar collectors are installed in a building, the daily sunshine hours of solar collectors should be larger than 4 h, the least sunshine hours specified by "Technical code of application of solar water heating systems in civil buildings" (GB 50364). To collect more annual radiation, solar collectors are usually installed on south-faced façade. However, for the region with site latitude less than 27°, the sunshine hours on the southern wall in the summer solstice are less than 4 h. As shown in Fig. 39, to make sunshine hours in the summer solstice longer than 4 h in the region with site latitude less than 27°, the wise way is to orient the wall 25–30° from the due south.

Potential solar water heating systems applicable in high buildings include individual system (domestic solar water heater), collective solar water heating and supply system, collective-individual hot water supply system, and domestic solar water heating system with collectors on the façade or balcony of buildings. Reasonable choice of system types should be done based on the roof area available for use,

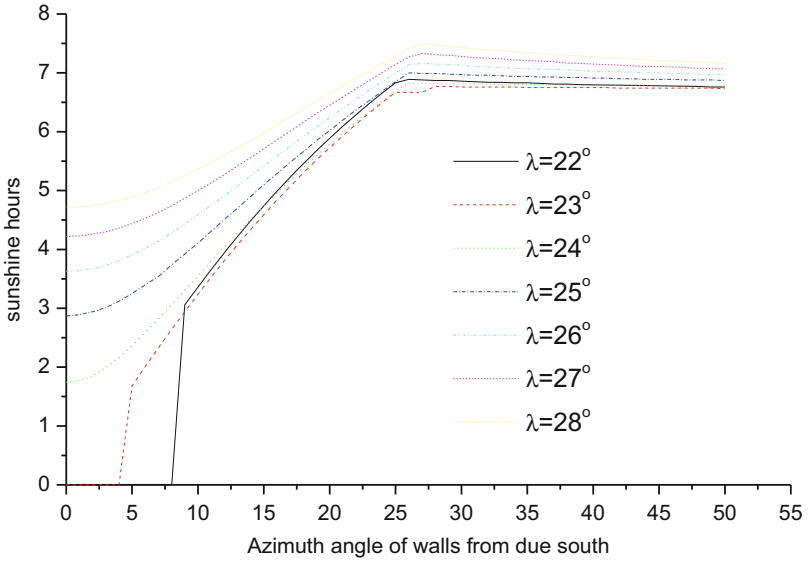

Fig. 39 Effects of azimuth angle of walls on sunshine hours in the summer solstice

height and orientation of buildings, building type, site latitude, as well as the requirements of house holders. If roof area is allowable, individual system is first advisable, followed by collective solar water heating system, and if roof area is not sufficient, collective heating systems or collective heating system in combination with domestic solar water systems with collectors on the façade or balcony can be preferably considered. The collective water heating but individual hot water storage and supply system is not preferably advisable in general due to high cost and low system efficiency resulting from long piping system and the use of heat exchanger in storage tanks located at each house. Typical illustrative projects are shown in Figs. 40 and 41. It should be noted that, to efficiently employ limited roof area for hot water supply in high buildings, flat-plate collectors are advisable because the annual collectible radiation on unit area of flat-plate collectors are 30% higher than evacuated tube solar collectors as seen in Table 3.

Economic Analysis on Solar Water Heating Systems Used in Kunming of China

Price of energy generated by solar water heating system is of importance to determine whether it is economically attractive compared with conventional water heaters. The price of the heat from a solar water heating system is determined by initial investment, life span, annual solar gain, and banking interest. As a case study, a comparison of heat price from a solar water system with collector area of 2.5 m^2 and daily efficiency of 45% to that from electrical water heaters and gas water

Fig. 40 Collective hot water supply systems. *Left*: collectors on roof, *right*: part of collectors on southern wall

Fig. 41 The collective system on the roof supplies hot water to north-faced houses, and domestic solar water heaters in balconies provide the hot water to south-faced houses

heaters is performed. In this comparison, assuming that the solar water heater with life span of 10 years is south-faced with the tilt angle of 25° (site latitude of Kunming) from the horizon (the annual radiation on the collector surface is about 6200 MJ/m^2) and electric resistance as the auxiliary heater, the annual banking interest is 3%, the price of electricity is 0.58 RMB/kWh (1 US dollar is about 6.4 RMB), and the gas obtained by gasifying coal is 1.6 RMB/m^3 in price and 4.6 kWh/m^3 in burning heat. In addition, efficiencies of electric water heater and gas water heater are assumed to be 90% and 85%, respectively, and the initial investment of electric heater and gas heaters is assumed to be 1500 RMB and 1800 RMB (current market price), respectively. The annual maintenance expense of all three water heaters is assumed to be 2% of the initial investment.

As shown in Table 4, compared to electric heaters and gas heaters, the solar water heater is economically attractive only if the cost of solar water heaters is less than 5000 RMB. Among all types of solar systems, the cost of collective-individual system is the highest (6000–8000 RMB), followed by domestic solar water heaters

Table 4 Comparison of price of the heat provided by three water heaters (RMB/kWh)

Init. Invest. (RMB)	Solar heater	Elec. heater	Gas heater
1000	0.1314	0.7811	0.4221
1500	0.1640	0.7811	0.4221
2000	0.1967	0.7811	0.4221
2500	0.2294	0.7811	0.4221
3000	0.2620	0.7811	0.4221
3500	0.2947	0.7811	0.4221
4000	0.3274	0.7811	0.4221
4500	0.3600	0.7811	0.4221
5000	0.3927	0.7811	0.4221
5500	0.4254	0.7811	0.4221
6000	0.4580	0.7811	0.4221
6500	0.4907	0.7811	0.4221
7000	0.5234	0.7811	0.4221
7500	0.5560	0.7811	0.4221
8000	0.5887	0.7811	0.4221

with collectors on the façade or balcony (3500–5000 RMB), the cost of collective solar heating systems is about 2000–2500 RMB, and the cost of domestic solar water heaters installing on the roof of buildings, dependent on material of water storage tank, is in between 2000 and 3000 RMB. This shows that solar water heaters are more economically attractive compared to conventional heaters in Kunming except the collective-individual solar systems.

Conclusions

The analysis in this chapter shows that the performance of flat-plate solar collectors is related to structure and materials used, and the performance of solar tube collectors is mainly affected by tube distance between two adjacent tubes, collector type, tilt-angle, and use of diffuse reflectors. For flat-plate collectors, the optimal orientation is south-faced and tilted at the site latitude for maximizing the annual radiation collection, whereas for solar tube collectors, the optimal tilt-angle of north-south tube arrays (T-type collector) is slightly less than site latitude, and that of horizontally arranged tube array is about 10–20 lower the site latitude in order to ensure more sky diffuse radiation. Compared to solar tube collectors, plate-flat collectors annually collect about 30% more radiation. Analysis shows that design of solar water heating system should be done based on demand of solar water and roof area allowable for the installation of solar collectors, and passive individual or collective solar water heating systems are preferable to be considered. Economic analysis indicates that solar water heating system is much attractive compared to electric and gas heaters.

Recently, the design of solar water heating systems is usually performed after the construction of buildings being finished, and the concept of building integration of solar system should be addressed in future, making the design and installation of solar water system in the same step as the design and construction of buildings where solar water heating system is required for hot water supply. In addition, solar collectors as building elements should be developed to meet the integration of solar water systems with buildings.

References

1. Hollands KGT, Unny TR, Raithby GD, Konicek L (1976) Free convection heat transfer across vertical fluid layers. J Heat Transf 98:189
2. Duffie JA, Beckmann WA (1991) Solar engineering of thermal processes, 2nd edn. Wiley, New York
3. Watmuff JH, Charters WWS, Procyor D (1977) Solar and wind induced external coefficients for solar collectors. Comples 2:56
4. Tang RS, Etzion Y, Meir IA (2004) Estimates of clear night sky emissivity in the Negev Highlands, Israel. Energy Convers Manag 45:1831–1843
5. Tang RS, Sun ZG, Li ZM, YM Y, Zhong H, Xia CF (2008) Experimental investigation on the thermal performance of flat-plate collectors at night. Energy Convers Manag 49:2642–2646
6. Xu DL, Tang RS, Cheng YB (2013) Sky emissivity at clear nights in Yunnan, China. Appl Mech Mater 291–294:96–100
7. Berdahl P, Fromberg R (1982) The thermal radiance of clear skies. Sol Energy 29:299–314
8. Berdahl P, Martin M (1984) Emissivity of clear skies. Sol Energy 32:663–664
9. Cook J (1985) Passive cooling. The MIT Press, Cambridge, MA/London
10. Tang RS, Etzion Y (2004) Comparative studies on water evaporation rate from a wetted surface and that from a free water surface. Build Environ 39:77–86
11. Incropera FP, Dewitt DP (1996) Fundamentals of heat transfer. Wiley, New York/Toronto et al
12. Berger X, Buriot D, Garnier F (1984) About the equivalent radiative temperature for clear skies. Sol Energy 32:725–733
13. Klein SA (1975) Calculation of flat-plate loss coefficient. Sol Energy 19:79
14. Zhang QC (2000) Recent progress in high-temperature solar selective coatings. Sol Energy Mater Sol Cells 62:63–74
15. Liu XY, Tang RS (2013) Design optimization of SS-AlN cermet solar selective coatings. Appl Mech Mater 260–261:40–45
16. Rabl A (1985) Active solar collectors and their applications. Oxford University Press, Oxford
17. Tang RS, Gao WF, Yu YM, Chen H (2009) Optimal tilt-angle of all-glass evacuated tube solar collectors. Energy 34:1387–1395
18. Collares-Pereira M, Rabl A (1979) The average distribution of solar radiation: correlations between diffuse and hemispherical and between hourly and daily insolation values. Sol Energy 22:155–164
19. Tang RS, Wu T (2004) Optimal tilt-angles for solar collectors used in China. Appl Energy 79:239–248
20. Bruce AW, Charles SB (1977) Freeze protection for flat-plate collector using heating. Sol Energy 19:745–746
21. Salasovich J, Burch J, Barker G (2002) Geographic constraints on passive domestic hot water systems due to pipe freezing. Sol Energy 73:469–474
22. Tang RS, Cheng YB, MG W, Li ZM, YM Y (2010) Experimental and modeling studies on thermosiphon domestic solar water heaters with flat-plate collectors at clear nights. Energy Convers Manag 51:2548–2556

23. Huang BJ, Hsieh CT (1985) A simulation method for solar thermosyphon collector. Sol Energy 35:31–43
24. Morrison GL (1980) Transient response of thermosyphon solar collectors. Sol Energy 24:55–61
25. Ong KS (1974) A finite-difference method to evaluate the thermal performance of solar water heater. Sol Energy 18:137–147
26. Close DJ (1962) The performance of solar water heaters with natural circulation. Sol Energy 6:33–40
27. Huo ZC, Yan XB, Zhang L (1991) Experimental study on N-S oriented all-glass evacuated tube by visual technique and its practical system design. Acta Energiae Solaris Sinica 12:412–417. (in Chinese with English abstract)
28. Tang RS, Yang YQ, Gao WF (2011) Comparative studies on thermal performance of water-in-glass evacuated tube solar heaters with different collector tilt-angles. Sol Energy 85:1381–1387
29. Yang YQ, Tang RS (2014) Effects of tube space on the thermal performance of water-in-glass evacuated tube solar water heaters. Adv Mater Res 860–863:81–87
30. Tang RS, Yang YQ (2014) Nocturnal reverse flow in water-in-glass evacuated tube solar water heaters. Energy Convers Manag 80:173–177
31. Shah LJ, Furbo S (2007) Theoretical flow investigations of an all glass evacuated tubular collector. Sol Energy 81:822–828
32. Tang RS, Liu NY (2012) Shading effect and optimal tilt-angle of collectors in a collector array. Adv Mater Res 588–589:2078–2082
33. Dunkle RV, Davey ET (1970) Flow distribution in absorber banks. presented at Melbourne international solar energy society conference. GB50364-2005. Technical code of application of solar water heating systems in civil buildings, issued by National Technology Supervision Bureau in 2005 (in Chinese)